JBC ARTICLE

Insulin signaling requires glucose to promote lipid anabolism in adipocytes

Received for publication, June 18, 2020, and in revised form, July 14, 2020 Published, Papers in Press, July 28, 2020, DOI 10.1074/jbc.RA120.014907

James R. Krycer[1,2], Lake-Ee Quek[2,3], Deanne Francis[1,2], Armella Zadoorian[1,2], Fiona C. Weiss[1,2], Kristen C. Cooke[1,2], Marin E. Nelson[1,2], Alexis Diaz-Vegas[1,2], Sean J. Humphrey[1,2], Richard Scalzo[4], Akiyoshi Hirayama[5,6], Satsuki Ikeda[5], Futaba Shoji[5], Kumi Suzuki[5], Kevin Huynh[7], Corey Giles[7], Bianca Varney[2,8], Shilpa R. Nagarajan[2,8], Andrew J. Hoy[2,8], Tomoyoshi Soga[5,6], Peter J. Meikle[7], Gregory J. Cooney[2,8], Daniel J. Fazakerley[1,2], and David E. James[1,2,8,*]

From the [1]School of Life and Environmental Sciences, the [2]Charles Perkins Centre, the [3]School of Mathematics and Statistics, the [4]Faculty of Engineering and Information Technologies, and the [8]Sydney Medical School, University of Sydney, Sydney, New South Wales, Australia, the [5]Institute for Advanced Biosciences, Keio University, Tsuruoka, Yamagata, Japan, [6]AMED-CREST, Japan Agency for Medical Research and Development (AMED), Otemachi, Chiyoda-Ku, Tokyo, Japan, and the [7]Baker Heart and Diabetes Institute, Melbourne, Victoria, Australia

Edited by Qi-Qun Tang

Adipose tissue is essential for metabolic homeostasis, balancing lipid storage and mobilization based on nutritional status. This is coordinated by insulin, which triggers kinase signaling cascades to modulate numerous metabolic proteins, leading to increased glucose uptake and anabolic processes like lipogenesis. Given recent evidence that glucose is dispensable for adipocyte respiration, we sought to test whether glucose is necessary for insulin-stimulated anabolism. Examining lipogenesis in cultured adipocytes, glucose was essential for insulin to stimulate the synthesis of fatty acids and glyceride–glycerol. Importantly, glucose was dispensable for lipogenesis in the absence of insulin, suggesting that distinct carbon sources are used with or without insulin. Metabolic tracing studies revealed that glucose was required for insulin to stimulate pathways providing carbon substrate, NADPH, and glycerol 3-phosphate for lipid synthesis and storage. Glucose also displaced leucine as a lipogenic substrate and was necessary to suppress fatty acid oxidation. Together, glucose provided substrates and metabolic control for insulin to promote lipogenesis in adipocytes. This contrasted with the suppression of lipolysis by insulin signaling, which occurred independently of glucose. Given previous observations that signal transduction acts primarily before glucose uptake in adipocytes, these data are consistent with a model whereby insulin initially utilizes protein phosphorylation to stimulate lipid anabolism, which is sustained by subsequent glucose metabolism. Consequently, lipid abundance was sensitive to glucose availability, both during adipogenesis and in *Drosophila* flies *in vivo*. Together, these data highlight the importance of glucose metabolism to support insulin action, providing a complementary regulatory mechanism to signal transduction to stimulate adipose anabolism.

Adipose tissue represents a key metabolic hub, with dysregulated adipose lipid metabolism being common in the etiology of metabolic disorders such as insulin resistance (1, 2). Adipose metabolism responds dynamically to the nutritional milieu, storing energy as lipid under nutrient replete conditions and mobilizing lipid stores during fasting. This balance is tightly regulated by insulin, which, in response to rising blood glucose levels, suppresses lipolysis and promotes glucose uptake and utilization. Importantly, adipose glucose uptake becomes impaired early in the progression of insulin resistance in both rodents and humans (3–5). Furthermore, adipose-specific knockout of the insulin-responsive glucose transporter GLUT4 reportedly causes whole-body insulin resistance in mice (6). Therefore, how adipocytes metabolize glucose is essential to organismal metabolic homeostasis.

Upon insulin stimulation, the adipocyte markedly adapts its metabolism to cater for the substantial influx of glucose (7). To achieve this, insulin engages kinase signaling cascades to alter the phosphorylation of numerous metabolic proteins (8, 9). In adipocytes, this rapidly activates anabolic enzymes before glucose is taken up (9), implying that anabolism is preemptively stimulated. This pulls glucose flux down specific metabolic pathways because of an increase in substrate demand. A corollary of this model is that glucose metabolism fuels anabolism in adipocytes. This is supported by studies in rodent adipose explants and adipocytes, which demonstrated that lipogenesis occurs in the presence of glucose, which acts as a carbon source for fatty acid synthesis (10) and facilitates fatty acid esterification for lipid storage (11). However, these studies were typically performed in minimal media containing only glucose and/or fatty acids as substrates. Thus, the quantitative contribution of glucose to these lipogenic processes is unclear under more physiological circumstances, such as in the presence of other substrates like amino acids. This raises the possibility that glucose is sufficient, but not necessary, for insulin-stimulated lipid anabolism in adipose tissue.

In support of this, branched chain amino acids (BCAAs) also contribute substantially as lipogenic substrates in cultured adipocytes, as well as primary adipocytes and adipose tissue from rodents and humans (12–15). Likewise, we previously observed that glucose is not required for insulin to stimulate respiration in adipocytes (16), which relies on other carbon substrates when glucose is absent. Thus, although anabolic processes such

This article contains supporting information.

* For correspondence: David E. James, david.james@sydney.edu.au.
Present address for Daniel J. Fazakerley: Metabolic Research Laboratories, Wellcome Trust–Medical Research Council Institute of Metabolic Science, University of Cambridge, Cambridge, United Kingdom.

as lipogenesis may serve as a means of glucose storage in adipocytes, it is unclear whether glucose *per se* is necessary for insulin action. Insulin may stimulate anabolism predominantly by kinase signaling to activate key metabolic enzymes, with the adipocyte using alternate substrates (*e.g.* amino acids) in the absence of glucose. This is an important question to address given that insulin-resistant adipocytes have a selective impairment in glucose uptake (17), which may influence not only glucose disposal but also other arms of insulin action such as lipid storage if glucose is required for these processes.

Thus, we sought to clarify the role of glucose in insulin-stimulated anabolism and lipid storage in cultured adipocytes. We found that kinase signaling *per se* was unaffected by glucose availability, but glucose was required to be present for insulin to stimulate lipogenesis as an end point of kinase signaling. Metabolic tracing revealed that glucose metabolism provided both substrates and metabolic control to enable insulin to promote fatty acid and glyceride–glycerol synthesis. Importantly, glucose had no impact on lipogenesis in the absence of insulin, suggesting that basal and insulin-stimulated lipogenesis use distinct carbon sources. Furthermore, insulin could inhibit lipolysis independently of glucose, demonstrating that only a subset of insulin's actions was sensitive to glucose metabolism. This presents a model whereby protein phosphorylation occurs rapidly before glucose uptake (9) to stimulate anabolism, which is then sustained by subsequent glucose uptake and utilization. Consistent with a key role for glucose in lipid storage, lipid accumulation was sensitive to glucose availability in both adipocytes and *Drosophila* flies *in vivo*. Together, these data demonstrate that kinase signaling alone is insufficient, requiring glucose metabolism as a complementary regulatory mechanism to enable insulin to increase lipid anabolism in adipocytes.

Results

Glucose availability influences most, but not all, insulin-dependent changes in metabolism

In this study, we aimed to address the importance of glucose in insulin-stimulated lipid metabolism in adipocytes. Glucose metabolism can fuel anabolic processes through provision of carbon substrate, ATP, and NADPH (18) via specific pathways in central carbon metabolism. Thus, we initially assessed how metabolites in these pathways responded to insulin, with or without glucose. To achieve this, we utilized galactose, a hexose that enters glycolysis via a different pathway (Fig. 1*A*) and is metabolized more slowly than glucose, such that flux through anabolic pathways becomes dependent on nonglucose sources such as amino acids (19). We previously showed that substituting glucose for galactose in adipocytes abolished the increase in lactate production, but not respiration, in response to insulin (16). We anticipated that if glucose was required for anabolism, flux through anabolic pathways would increase in response to insulin stimulation, but the metabolites in these pathways would become depleted if glucose was substituted with galactose.

Cultured adipocytes were incubated with either (i) glucose alone, (ii) insulin and glucose, or (iii) insulin and galactose. Following treatment, cell lysates were subjected to targeted metabolomics analysis. Visualizing the variation in total metabolite abundance by principal-component analysis revealed that the samples from the glucose/insulin condition were clustered away from the glucose/control condition (Fig. 1*B*), implying that insulin causes substantial variation in the metabolome when glucose was available. Replacing glucose with galactose (galactose/insulin) generated a cluster closer to glucose/control, in the opposite direction to glucose/insulin, demonstrating that glucose availability altered the effect of insulin on the metabolome.

Focusing on individual metabolites in central carbon metabolism revealed that insulin increased the total abundance of most nonamino acid metabolites (Fig. 1*C*, *x axis*), but these changes were dependent on the presence of glucose (Fig. 1*C*, *y axis*). This glucose dependence was exemplified by metabolites in glycolysis, the pentose phosphate pathway, and lipogenesis (Fig. 1*D*, *top panel*).

In these experiments, glucose and galactose were ^{13}C-labeled to allow us to determine whether these sugars were a direct substrate for metabolites or glucose acted indirectly via metabolic control (*e.g.* influencing mass action or the levels of an allosteric regulator) to support insulin-stimulated metabolism. These labeled sugars did not alter total metabolite abundances when compared with incubation with naturally labeled sugars (Fig. S1*A*). To demonstrate the utility of substrate labeling, we initially used these labeled sugars to verify the metabolism of galactose. We considered glucose 6-phosphate, the entry point of both sugars into glycolysis (Fig. 1*A*). The dominant isotopologue for glucose 6-phosphate was m6 (all six carbons are ^{13}C-labeled) for insulin-treated adipocytes incubated with either sugar (Fig. S1*B*), confirming that both sugars are taken up by adipocytes and enter glycolysis. However, ^{13}C-labeled levels of glucose 6-phosphate (Fig. S1*B*) and other metabolites (Fig. 1*D*, *bottom panel*) were substantially lower with galactose, confirming that galactose served as a poor substrate for central carbon metabolism (Fig. 1*A*). This concurs with previous observations in isolated rodent adipocytes, which showed that insulin stimulated the uptake of galactose similarly to glucose, but not downstream galactose metabolism (20).

We more closely examined isotopologue patterns to understand how glucose facilitated insulin-responsive metabolism (Fig. 1*E*). For instance, we observed that insulin required the presence of glucose to increase metabolites in glycolysis (Fig. 1*D*, *top panel*). For these metabolites, like glucose 6-phosphate, the dominant isotopologue in the glucose/insulin condition was maximally labeled (*e.g.* m6 for fructose 1,6-bisphosphate and m3 for phosphoenolpyruvate) (Fig. 1*E*, *top left panel*). Thus, glucose contributed most of the carbon to metabolites in glycolysis under insulin-stimulated conditions.

Tricarboxylic acid (TCA) cycle metabolites also increased with insulin, but this was not dependent on glucose (Fig. 1*E*, *bottom right panel*). Furthermore, although these metabolites were substantially labeled in the glucose/insulin condition, the dominant isotopologue was m0 (unlabeled) in the galactose/insulin condition, indicative of the use of nonglucose carbon. This suggests that glucose can facilitate the insulin-stimulated increase in TCA cycle metabolites, but alternate substrates such as amino acids (15, 21) can be utilized if glucose is absent.

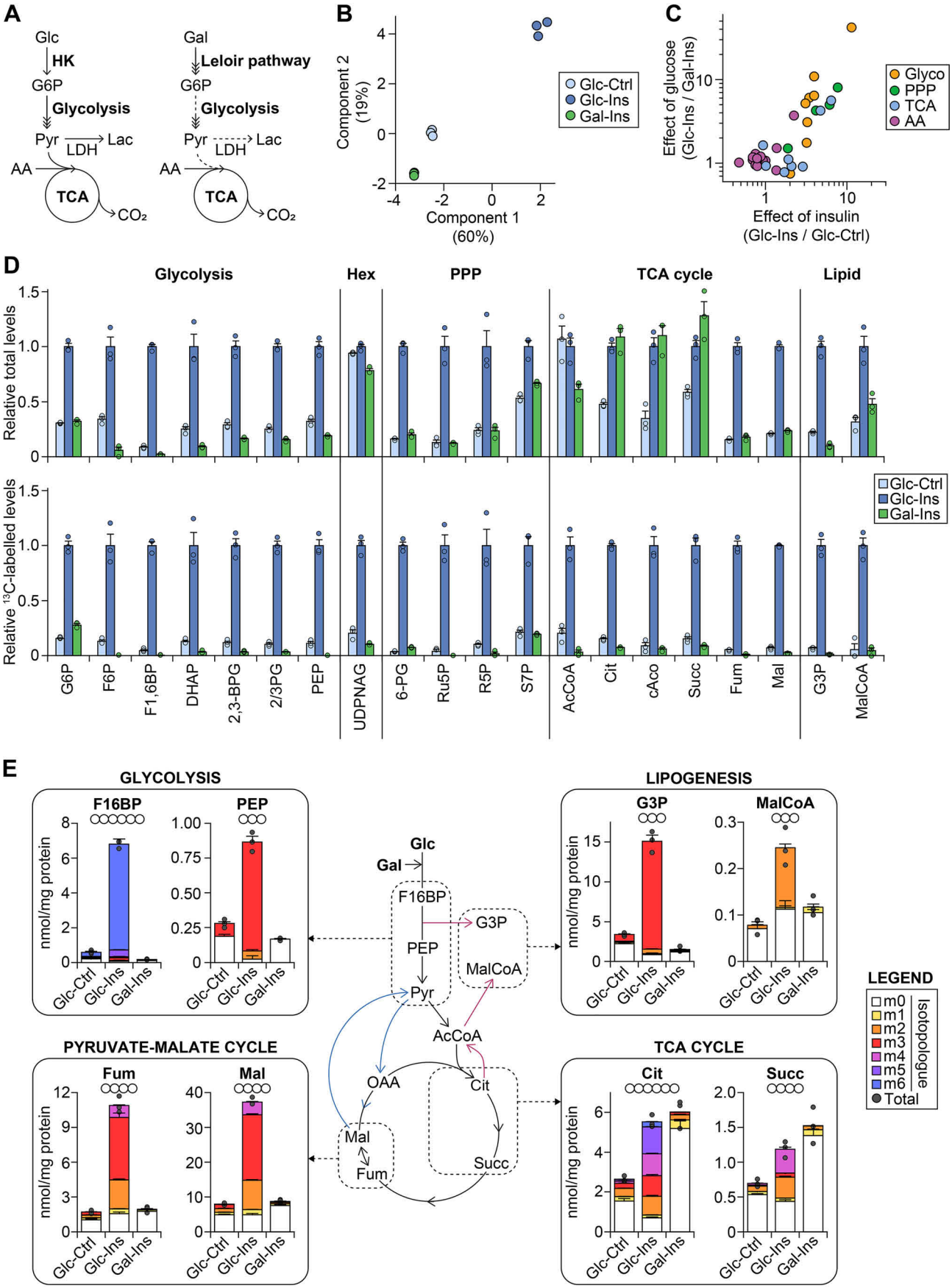
A
Glc
HK
G6P
Glycolysis
Pyr
LDH
Lac
AA
TCA
CO₂
Gal
Leloir pathway
B
Component 2 (19%)
Component 1 (60%)
Glc-Ctrl
Glc-Ins
Gal-Ins
C
Effect of glucose (Glc-Ins / Gal-Ins)
Effect of insulin (Glc-Ins / Glc-Ctrl)
Glyco
PPP
TCA
AA
D
Glycolysis
Hex
PPP
TCA cycle
Lipid
Relative total levels
Relative ¹³C-labelled levels
G6P
F6P
F1,6BP
DHAP
2,3-BPG
2/3PG
PEP
UDPNAG
6-PG
Ru5P
R5P
S7P
AcCoA
Cit
cAco
Succ
Fum
Mal
G3P
MalCoA
E
GLYCOLYSIS
F16BP
PEP
LIPOGENESIS
G3P
MalCoA
PYRUVATE-MALATE CYCLE
Fum
Mal
TCA CYCLE
Cit
Succ
nmol/mg protein
Glc
Gal
F16BP
G3P
PEP
MalCoA
Pyr
AcCoA
OAA
Cit
Mal
Fum
Succ
LEGEND
Isotopologue
m0
m1
m2
m3
m4
m5
m6
Total

This corroborates our previous observations that insulin-stimulated respiration did not require glucose (16). Interestingly, this did not apply to fumarate and malate, which, like glycolytic metabolites, increased with insulin treatment in a glucose-dependent manner (Fig. 1*E*, *bottom left panel*). Malate also participates in the pyruvate–malate cycle: pyruvate to oxaloacetate by pyruvate carboxylase, oxaloacetate to malate by malate dehydrogenase, malate to pyruvate by malic enzyme (Fig. 1*E*, *blue arrows*). This cycle generates the m3 isotopologue of malate, which was dominant only in the glucose/insulin condition (Fig. 1*E*). Thus, our data imply that the pyruvate–malate cycle responds to glucose metabolism, corroborating our previous observations that this cycle is tightly coupled to glycolysis (7). Together, this demonstrated that although insulin increased numerous metabolites, only selected pathways depended on the carbon provided by glucose to facilitate this response.

Insulin-stimulated lipogenesis is glucose-dependent

We next focused on lipogenic substrates, because recent studies (15) have reinvigorated the notion that nonglucose substrates may fuel a major portion of lipogenesis in adipocytes (12–14). Because we set out to determine the requirement for glucose in adipocyte lipogenesis, we considered the precursors to lipid synthesis and storage, malonyl-CoA and glycerol 3-phosphate (Fig. 1*E*, *top right panel*).

Insulin increased glycerol 3-phosphate (*G3P*) concentrations in a glucose-dependent manner, with the fully labeled (m3) isotopologue predominant in the glucose/insulin condition. Thus, with insulin stimulation, G3P was predominantly derived from exogenous glucose, which is intuitive because G3P is derived from glycolysis. Furthermore, the m0 isotopologue decreased upon insulin treatment, even without glucose present, suggesting that G3P is used in response to insulin and glucose is required to replenish G3P during insulin-stimulated anabolism.

Malonyl-CoA followed a similar pattern, with the rise in malonyl-CoA in the glucose/insulin condition being due to the m2 isotopologue (Fig. 1*E*, *top right panel*). Because malonyl-CoA is derived from carboxylation of the two-carbon carrier acetyl-CoA, the m2 isotopologue reflects lipogenic carbon sourced entirely from glucose. However, the m0 isotopologue did not decrease upon insulin stimulation. Together, this implies that insulin-responsive lipogenesis is glucose-dependent, and the contribution of malonyl-CoA from nonglucose sources is maintained regardless of insulin status.

Based on these observations, we examined how *de novo* lipogenesis responds to insulin treatment in the presence or absence of glucose. As an additional control to galactose, we included a "no sugar" condition, which, like galactose, abolished insulin-responsive lactate production (Fig. S2*A*). Furthermore, we reduced the sugar concentration in the medium from 25 to 10 mM, which is more physiological and enabled us to conserve labeled substrate. We assessed whether this would impact glucose incorporation into lipid; increasing the medium glucose concentration from 5 to 25 mM caused a ~2.5-fold increase in glucose uptake (22), but only increased glucose incorporation into fatty acid or glyceride–glycerol moieties by ~50% (Fig. S2*B*). This demonstrated that altering the sugar concentration should have little impact on glucose utilization in lipid metabolism.

De novo lipogenesis was measured by incubation with ^{3}H-labeled H_2O ($[^3H]H_2O$): the reduction reactions in *de novo* lipogenesis incorporate ^{3}H atoms into the backbone of fatty acids and glyceride–glycerol moiety, thus providing a measure of newly synthesized lipid (23, 24). This revealed that insulin-responsive synthesis of both glyceride–glycerol (Fig. 2*A*) and fatty acid (Fig. 2*B*) moieties was blunted in the absence of glucose. To test whether this was due to glucose acting as a carbon source, we incubated parallel adipocyte cultures with $[^3H]H_2O$ or [^{14}C]glucose, to assess total or glucose-derived lipid synthesis, respectively. Upon insulin treatment, the glyceride–glycerol moiety was almost entirely derived from exogenous glucose (Fig. 2*C*). Interestingly, the synthesis of fatty acids from glucose carbon increased with a similar magnitude to total synthesis, but this glucose-derived lipid only accounted for a portion of the total newly synthesized lipid (Fig. 2*D*). Thus, insulin-stimulated adipocytes derive lipogenic substrates from exogenous glucose carbon, but nonglucose sources also contribute substantially to fatty acid synthesis under these conditions.

We complemented these experiments with a stable-isotope lipidomics approach, in which we examined which lipid species were enriched by ^{13}C-glucose (Fig. S2*C*). We confirmed an insulin response by the increase in total and ^{13}C-enriched lactate production (Fig. S2*D*), as observed previously (22). Because the treatment/labeling period was short (1 h), we included a 48-h incubation period with ^{13}C- or naturally labeled glucose as positive and negative controls for detecting lipid isotopologues (Fig. S2*C*). We examined several lipid classes (Fig. 2*E*): although ^{13}C enrichment could be detected across all lipid classes after a 48-h labeling period, only acylglycerides (triacylglycerides

Figure 1. Glucose availability influences insulin-dependent changes in metabolism. *A*, schematic depicting the entry of glucose (*Glc*) and galactose (*Gal*) into central carbon metabolism. *B–E*, 3T3-L1 adipocytes were serum-starved in medium BS supplemented with 25 mM glucose for 1.5 h and then treated with (*Ins*) or without (control, *Ctrl*) 100 nM insulin for 1 h in medium BS supplemented with 25 mM [U-^{13}C]glucose or [U-^{13}C]galactose. Following treatment, intracellular metabolites were extracted and subjected to targeted metabolomics analysis. The data were obtained from three separate experiments. A subset of this data set has been published elsewhere (7). *B*, principal component analysis of total metabolite abundance, with individual data points shown. Percentages on the axes denote the fraction of variance in the metabolome explained by each component. *C*, effect of glucose and insulin on the total abundance of metabolites from selected metabolic pathways, derived from the ratio of the conditions indicated on the axes. Mean data points shown. *D*, total (*top panel*) and ^{13}C-labeled (*bottom panel*) metabolite abundance, expressed relative to glucose/insulin (*Glc-Ins*) condition. The data are presented as means ± S.E. (*error bars*). *E*, isotopologue abundance for selected metabolites. The *circles* beneath each metabolite name denote the number of labeled carbons considered for that metabolite. isotopologues are denoted by the number of ^{13}C-labeled carbons: for instance, m0 has no labeled carbons (*i.e.* is unlabeled), m1 has one ^{13}C-labeled carbon, m2 has two ^{13}C-labeled carbons, etc. The data are presented as means ± S.E. (*error bars*) for individual isotopologues and separate data points for total abundance. *2,3BPG*, 2,3-bisphosphoglycerate; *2/3PG*, 2- and 3-phosphoglycerate; *6-PG*, 6-phosphogluconate; *AA*, amino acid; *AcCoA*, acetyl-CoA; *cAco*, *cis*-aconitate; *Cit*, citrate; *DHAP*, dihydroxyacetone phosphate; *F1,6BP*, fructose 1,6-bisphosphate; *F6P*, fructose 6-phosphate; *Fum*, fumarate; *G6P*, glucose 6-phosphate; *Glyco*, glycolysis; *HK*, hexokinase; *Lac*, lactate; *LDH*, lactate dehydrogenase; *Mal*, malate; *MalCoA*, malonyl-CoA; *OAA*, oxaloacetate; *PEP*, phosphoenolpyruvate; *PPP*, pentose phosphate pathway; *Pyr*, pyruvate; *R5P*, ribose 5-phosphate; *Ru5P*, ribulose 5-phosphate; *S7P*, sedoheptulose 7-phosphate; *Succ*, succinate; *UDP-NAG*, uridine diphosphate N-acetylglucosamine.

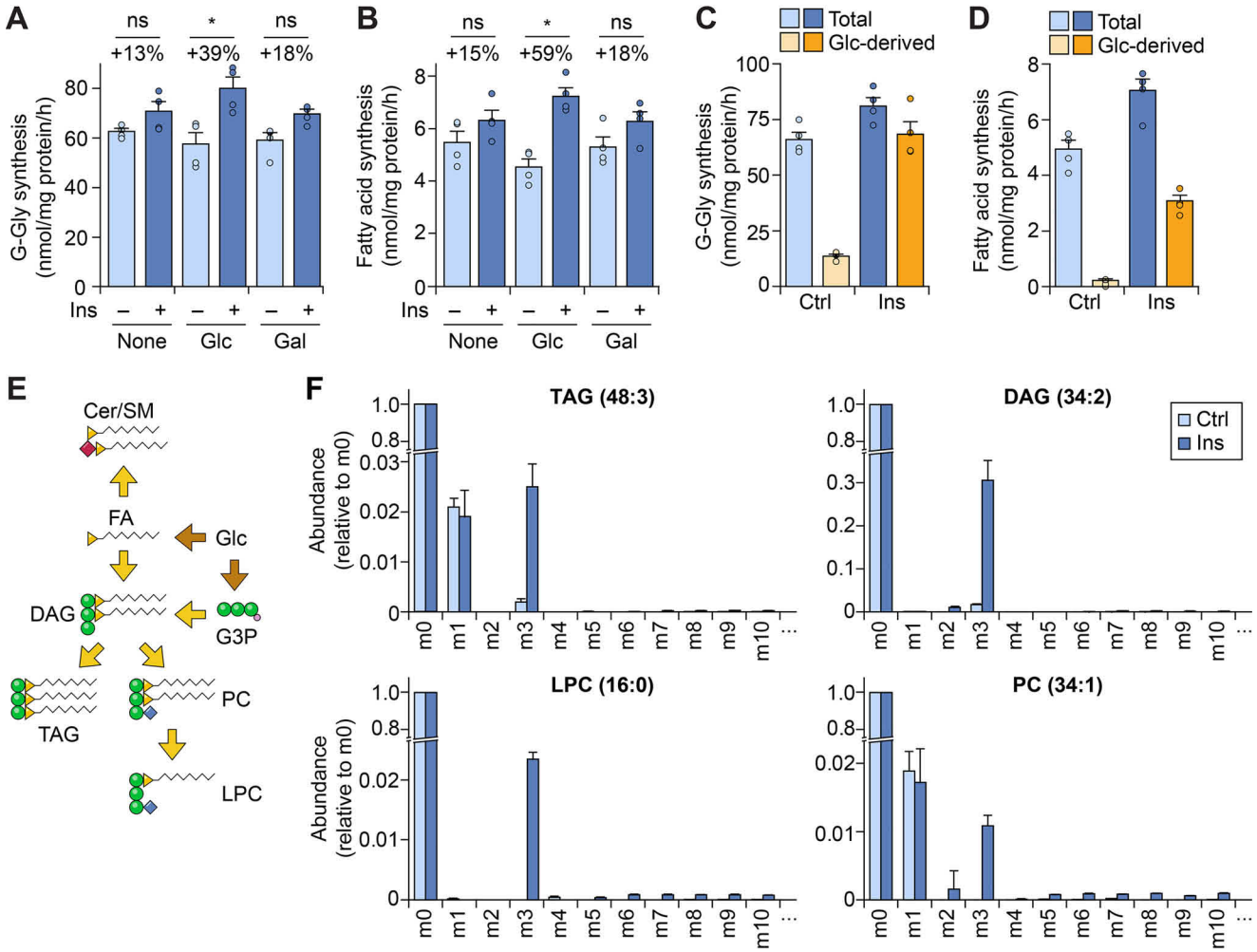

Figure 2. Insulin-stimulated lipogenesis is glucose-dependent. *A* and *B*, 3T3-L1 adipocytes were treated with or without 100 nM insulin (*Ins*) for 1 h, in medium C supplemented with 1 mCi/ml [^{3}H]H_2O and either no sugar (*None*) or 10 mM sugar (glucose, *Glc*; galactose, *Gal*). Following treatment, lipids were extracted and saponified, with radiotracer incorporation determining the synthesis rates of the glyceride–glycerol (*G-Gly*) (*A*) and fatty acid (*B*) moieties, as described under "Experimental procedures." The data are presented as means ± S.E. (*error bars*), from four separate experiments. The percentages above the data columns denote the change relative to the respective "no insulin" condition. *, $p < 0.05$; *ns*, $p > 0.05$ (not significant), by two-sample *t* test. *C* and *D*, 3T3-L1 adipocytes were treated with or without insulin for 1 h (*Ctrl*, control: no insulin), in medium C supplemented with 10 mM glucose. The media were also supplemented with radiotracer, either 1 mCi/ml [^{3}H]H_2O or 2 μCi/ml [U-^{14}C]glucose, in parallel cultures. Following treatment, the lipids were extracted and saponified, with radiotracer incorporation determining the rate of total ([^{3}H]H_2O tracer) or glucose-derived ([^{14}C]glucose tracer) synthesis of G-Gly (*C*) or fatty acid (*D*) moieties, as described under "Experimental procedures." The data are presented as means ± S.E. (*error bars*) from four separate experiments. *E*, schematic depicting the synthesis of different lipid species from glucose. *Cer/SM*, ceramide/sphingomyelin; *DAG*, diacylglyceride; *FA*, fatty acid; *LPC*, lysophosphatidylcholine; *PC*, phosphatidylcholine. *F*, 3T3-L1 adipocytes were treated with or without 100 nM insulin for 1 h in medium C, supplemented with 10 mM [U-^{13}C]glucose. These conditions were a subset of a larger experiment, detailed in Fig. S2C. Following treatment, the lipids were extracted and subjected to targeted lipidomics analysis. For the representative lipids shown, isotopologue abundances were made relative to the m0 isotopologue for each condition. The data are presented as means ± S.D. (*error bars*) from three biological replicates.

(TAGs) and diacylglycerides) and phospholipids (lysophosphatidylcholine and phosphatidylcholine) exhibited detectable enrichment that increased after 1 h of insulin treatment (Fig. S2*E*). If glucose is incorporated into the fatty acid moiety, this would generate m2/m4/m6/etc isotopologues. These isotopologues were substantially less abundant than the m3 isotopologue (Fig. 2*F*), which represents the glyceride–glycerol backbone in these lipid species. The absence of a dominant m3 isotopologue for ceramide (Fig. S2*F*), which lacks the glyceride–glycerol backbone, supports this interpretation. This corroborates the prominent role that glucose plays in the synthesis of the glyceride–glycerol backbone, implied by our radiotracer experiments (Fig. 2*C*). Overall, these experiments demonstrate that glucose supports insulin-stimulated *de novo* lipogenesis by acting directly as a carbon substrate, contributing partially to fatty acid synthesis and being the dominant substrate for the glyceride–glycerol backbone across multiple lipid species.

Glucose displaces BCAAs as a lipogenic substrate

Because a large portion of the carbon for *de novo* fatty acid synthesis was not derived from glucose (Fig. 2*D*), we considered whether glucose metabolism influences lipogenesis indirectly, *i.e.* promotes lipogenesis from other carbon sources. For instance, malic enzyme (pyruvate–malate cycle, Fig. 1*E*) and the pentose phosphate pathway are both NADPH sources, and flux through these pathways was highly glucose-dependent (Fig. 1, *D* and *E*); hence, glucose metabolism may generate NADPH to facilitate lipogenesis. Given that BCAAs are a major lipogenic substrate in

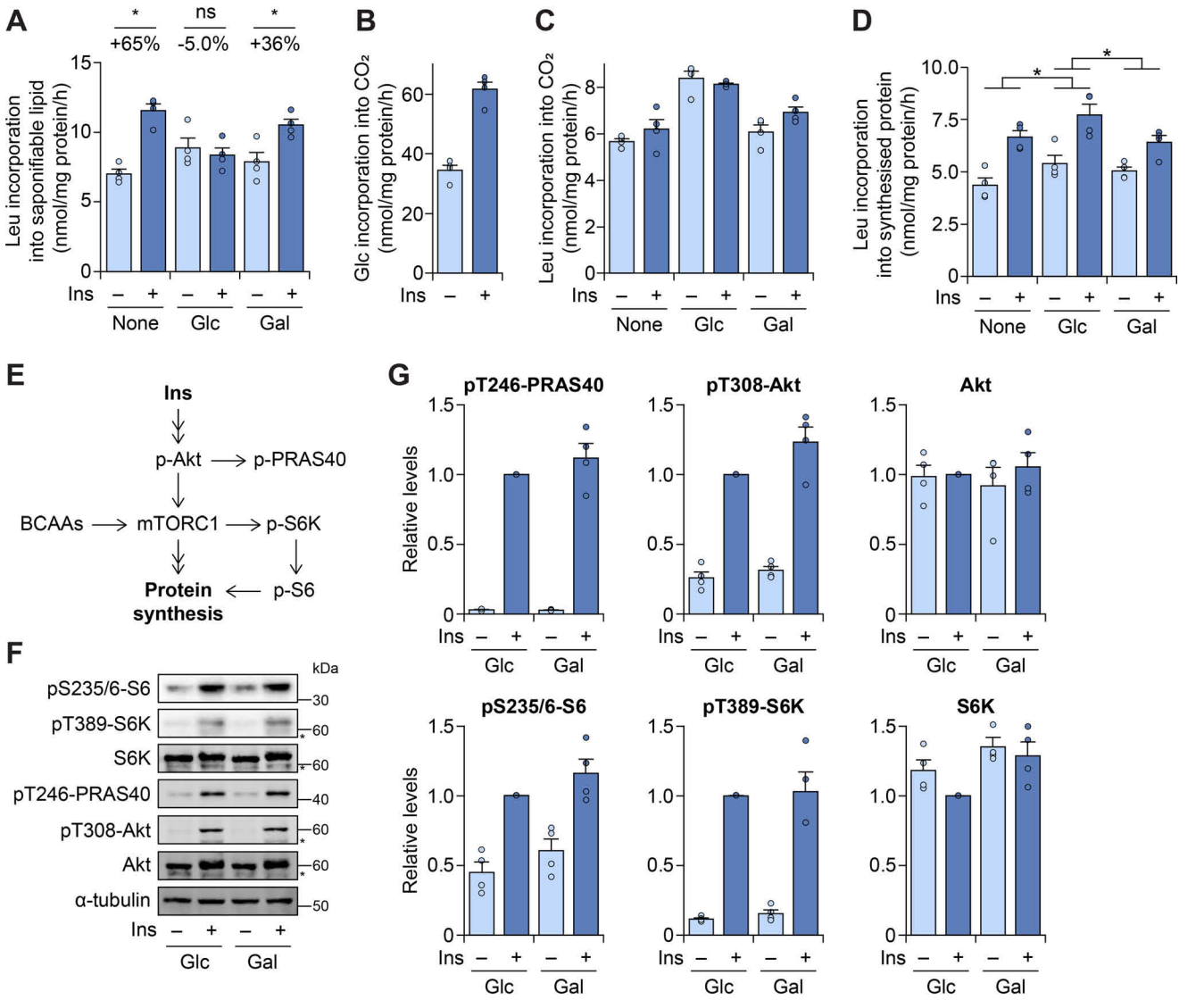

Figure 3. Glucose displaces leucine as a lipogenic substrate. *A*, 3T3-L1 adipocytes were treated with or without 100 nM insulin (*Ins*) for 1 h in medium C, supplemented with 0.5 μCi/ml L-[U-^{14}C]leucine and either no sugar (*None*) or 25 mM sugar (glucose, *Glc*; galactose, *Gal*). Following treatment, the cells were washed with cold PBS on ice before lysis with 1 M KOH. The lysates were subjected to saponification, and saponifiable lipids were extracted as described under "Experimental procedures." Leucine (*Leu*) incorporation into the saponifiable lipid fraction was determined by liquid scintillation counting. The data are presented as means ± S.E. (*error bars*) from four separate experiments. The percentages above the data columns denote the change relative to the respective "no insulin" condition. *, $p < 0.05$; *ns*, $p > 0.05$ (not significant), by two-sample *t* test. *B* and *C*, 3T3-L1 adipocytes were treated with or without 100 nM insulin for 1 h in medium C, supplemented with 25 mM glucose (*B*) or 25 mM sugar as indicated (*C*). The media were also supplemented with either 2 μCi/ml [U-^{14}C]glucose (*B*) or 0.5 μCi/ml L-[U-^{14}C]leucine (*C*) radiotracer, in parallel cultures. Substrate incorporation into CO_2 (*i.e.* substrate oxidation) was measured as described under "Experimental procedures." The data are presented as means ± S.E. (*error bars*) from four separate experiments. *D*, 3T3-L1 adipocytes were treated as described in *A*, except parallel cultures were cotreated with 5 μM cycloheximide as described under "Experimental procedures." Following treatment, protein was isolated by acetone precipitation, and leucine incorporation into the (newly synthesized) protein was determined by liquid scintillation counting. The data are presented as means ± S.E. (*error bars*) from four separate experiments. *, $p < 0.05$, effect of sugar assessed by two-way analysis of variance. *E*, schematic depicting the kinase signaling cascade by which insulin stimulates protein synthesis. *F*, 3T3-L1 adipocytes were treated as described in *A*, without radiotracer. Following treatment, the cells were harvested, and lysates were subjected to Western blotting. The blots shown are representative of four separate experiments. Nonspecific bands denoted by *asterisks*. *G*, quantification of protein levels from *F*, normalized to α-tubulin and made relative to the Glc/Ins condition. The data are presented as means ± S.E. (*error bars*) from four separate experiments.

adipocytes (12–15), we tested whether glucose supports lipogenesis from leucine. Surprisingly, insulin-stimulated incorporation of leucine into lipid was abolished by the presence of glucose (Fig. 3*A*), suggesting that glucose displaced leucine as a lipogenic substrate.

Consequently, we examined whether this displacement effect occurred with other aspects of leucine metabolism. Although insulin stimulated glucose oxidation (Fig. 3*B*), the presence of glucose slightly increased leucine oxidation regardless of insulin stimulation (Fig. 3*C*). We also assessed protein synthesis, using an optimized protocol based on acetone precipitation (Fig. S3, *A* and *B*), finding that the presence of glucose promoted leucine incorporation into newly synthesized protein (Fig. 3*D*). As a control, we determined whether glucose availability influenced insulin signaling to protein synthesis (Fig. 3*E*). This is mediated by the mTORC1 complex, which also requires BCAAs for activation (Fig. 3*E*). The total abundances of BCAAs decreased with both insulin treatment and replacing glucose with galactose, with the

former having a greater effect (Fig. S3*C*). However, this was not sufficient to impact kinase signaling, as assessed by Western blotting for phosphorylation of Akt and mTORC1 kinase substrates (Fig. 3, *E*, *F*, and *G*). Furthermore, cycloheximide, a protein synthesis inhibitor that provided baseline rates in the protein synthesis assay (Fig. 3*D*), did not affect insulin-dependent glucose metabolism (Fig. S3*D*).

Together, these results suggest that glucose diverted leucine from lipogenesis to oxidation and protein synthesis. Thus, glucose repartitioned leucine upon insulin stimulation.

Glucose is essential for suppression of fatty acid oxidation, but not lipolysis

Having demonstrated that glucose is essential for insulin-stimulated anabolism, particularly lipogenesis, we next considered how glucose influences lipid breakdown (Fig. 4*A*). For instance, it is known that active lipogenesis impairs fatty acid oxidation by inhibition of mitochondrial fatty acid import via malonyl CoA (25), which increased in a glucose-dependent manner (Fig. 1*E*). Thus, as expected, insulin required exogenous glucose to suppress fatty acid oxidation (Fig. 4*B*). Furthermore, glucose alone suppressed fatty acid oxidation (Fig. 4*B*).

Consequently, we hypothesized that glucose-dependent lipogenesis may also impair net lipolysis, at least by mass action resulting from decreased fatty acid oxidation and increased fatty acid synthesis and esterification. This would provide an additional mechanism for insulin to regulate lipolysis independently of kinase signaling (Fig. 4*A*). We considered lipolysis with or without stimulation by the β_3-adrenergic receptor agonist CL 316,243. To maximize effect size, we performed experiments using Krebs–Ringer phosphate (KRP) buffer, a minimal medium, supplemented with (25 mM) glucose as the only substrate. First, we confirmed that glucose did not influence the kinase signaling that regulates lipolysis by Western blotting for Akt (Fig. 4*C* and Fig. S4*A*) and protein kinase A (Fig. 4*C* and Fig. S4*B*) substrates. We next assessed lipolysis directly by measuring glycerol release into the medium, which revealed that glucose blunted insulin-stimulated anti-lipolysis (Fig. 4*D*). This appeared to be driven by a glucose-dependent increase in glycerol release with insulin treatment, possibly generated by dephosphorylation of G3P (26), a metabolite that increased with insulin in a glucose-dependent manner (Fig. 1*E*). Thus, we also measured fatty acid release, upon which the presence of glucose had no effect (Fig. 4*E*). To exclude the possibility that free fatty acids might be rerouted to oxidation in the absence of glucose (Fig. 4*B*) rather than released into the medium, we utilized triacsin C, a fatty acyl CoA synthase inhibitor, to inhibit fatty acid esterification (Fig. 4*F* and Fig. S4*C*), oxidation (Fig. 4*G*), and uptake (Fig. S4*D*). Triacsin C increased fatty acid release as expected (Fig. 4*H*), yet glucose had little effect on insulin-stimulated suppression of lipolysis when assessed by fatty acid (Fig. 4*H*) or glycerol (Fig. S4*E*) release. Together, these data demonstrate that glucose is required for the regulation of fatty acid oxidation, but not lipolysis.

Lipid storage is sensitive to glucose metabolism

Our data so far demonstrate that glucose availability influences insulin-dependent regulation of central carbon metabolism (Fig. 1), particularly the stimulation of lipid anabolism (Fig. 5*A*). Consequently, we hypothesized that adipocyte glucose metabolism would be vital for net lipid storage. Initially, we tested this by examining lipid accumulation during adipocyte differentiation *in vitro*. It has been previously reported that adipocyte differentiation is sensitive to varying glucose concentrations at the start of differentiation (27, 28). Here, we also manipulated the glucose content of the medium on the third day of differentiation (Fig. 5*B*), when the differentiation mixture was replaced with culture medium supplemented with insulin to trigger lipid accumulation. Removing glucose at this time point was sufficient to prevent lipid accumulation during adipogenesis (Fig. 5, *C* and *D*).

Next, we examined the importance of glucose metabolism on whole-body lipid storage. As a proof-of-principle experiment, we utilized *Drosophila*, which permit rapid organ-specific genetic manipulation and high-throughput metabolic studies (29). To block glucose metabolism via glycolysis, we knocked down two hexokinase isoforms, HexA and HexC (Fig. 5*E*). We knocked these genes down specifically in the fly fat body: HexC is the dominant isoform in the fat body of adult flies, whereas HexA is predominantly expressed in the fat body of fly larvae (FlyBase) (30). The fat body serves as both the adipose tissue and liver in flies, and because both are lipogenic tissues, any differences observed here would support the importance of glucose metabolism in whole-body lipid storage. These flies were fed diets that were supplemented with (i) glucose, (ii) fat (lard), or (iii) both. Importantly, the supplementation with glucose or fat provided similar energy content per g of food (see "Experimental procedures"), with thus roughly double the energy provided when both were present. Dietary glucose would stimulate the secretion of insulin-like peptides, the fly homolog of insulin (31, 32). Thus, if insulin(-like peptide) was required for lipid storage, but glucose metabolism was not, then we would expect lipid content to increase with the provision of dietary glucose (increased "insulin") and this would be unaffected by hexokinase knockdown (decreased glucose metabolism).

In control flies, the diets with glucose or both glucose and fat increased lipid content to levels higher than the diet with fat alone, suggesting that glucose alone was sufficient to raise lipid content (Fig. 5*F*). This effect of glucose on lipid storage was abolished by fat body-specific knockdown of HexC (HexC-KD), but not HexA (HexA-KD) (Fig. 5*F*). This is expected because HexA is not highly expressed in the fat body of adult flies (FlyBase) (30). Thus, whole-body lipid levels were sensitive to both dietary glucose and glucose metabolism specifically in the fat body.

Following 10 days on these diets, the flies were subjected to a starvation-resistance assay, which measures nutrient storage (during feeding) and utilization (during starvation). Prefeeding with diets supplemented with glucose promoted starvation resistance, and this was reversed by HexC-KD (Fig. 5*G*). As observed previously (33, 34)[9], there was a strong correlation between TAG storage during feeding and subsequent starvation resistance (Fig. 5*H*), suggesting that this starvation phenotype was due to differences in nutrient storage rather than

[9] D. Francis, S. Ghazanfar, E. Havula, J. R. Krycer, A. Senior, A. Y. Minard, T. Geddes, F. Weiss, J. Stoeckli, J. H. Y. Yang, and D. E. James, unpublished observations.

utilization. Together, this demonstrates that glucose metabolism in the fly fat body promoted whole-body lipid storage and associated resistance to starvation.

Discussion

In this study, we defined several essential roles for glucose in insulin-responsive metabolism in adipocytes. Glucose was required for most changes in the metabolome upon insulin stimulation (Fig. 1). This included pathways that provided carbon substrate and cofactors for lipid anabolism (Fig. 1), making glucose necessary for insulin-responsive lipogenesis (Fig. 2). Glucose was also needed for insulin to exert metabolic control, including the suppression of fatty acid oxidation (Fig. 4) and repartitioning of the lipogenic substrate, leucine, to CO_2 and protein synthesis (Fig. 3). In contrast, glucose was not required

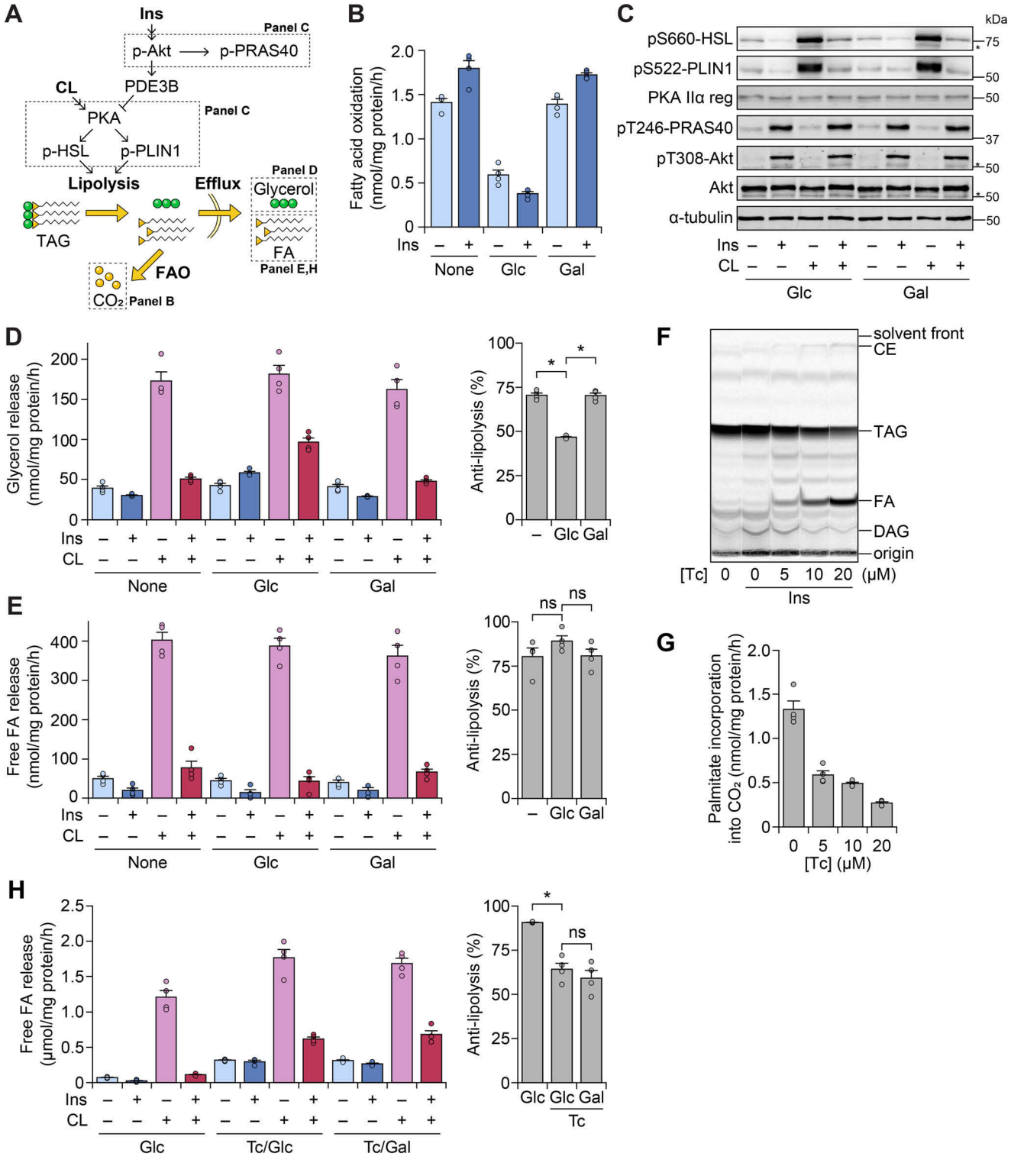

for insulin-dependent kinase signaling to suppress lipolysis (Fig. 4). Overall, glucose was required for lipid accumulation (Fig. 5*A*), both during adipogenesis and at the organismal level in *Drosophila* flies (Fig. 5). This dovetails with recent studies demonstrating that other carbon sources can generate lipogenic precursors (15, 35), with our study demonstrating that glucose is not only sufficient but is also necessary for insulin-responsive lipid metabolism. Together, these data uncover a requirement for glucose metabolism as a complementary means of regulating adipocyte anabolism in addition to insulin-dependent kinase signaling.

We primarily used 3T3-L1 adipocytes, which share many important features with primary adipocytes that are relevant to this study. Both are highly sensitive to insulin, responding with similar temporal kinetics; for instance, glucose uptake is stimulated substantially faster than protein synthesis (9, 36). Insulin stimulates lipogenesis and blocks lipolysis (Figs. 2 and 4) (10, 23, 37–39), with the increase in glucose incorporation into lipid (Fig. 2) similar in magnitude to primary adipocytes (37, 38). Furthermore, other substrates such as BCAAs contribute to fatty acid synthesis (Fig. 3) (12–15). Lastly, other glucose-utilizing pathways can function independently of exogenous glucose, such as lactate production and respiration (16, 22). Thus, 3T3-L1 adipocytes possessed the necessary metabolic features to test the necessity for glucose metabolism in insulin-stimulated lipid metabolism, and this relationship is likely translatable to primary adipocytes.

Our survey of adipocyte central carbon metabolism revealed a disconnect between glycolysis and the TCA cycle in adipocytes in terms of their glucose dependence. For instance, insulin required glucose as a carbon substrate to increase the abundance of metabolites in stimulated glycolysis, as well as the pentose phosphate pathway and pyruvate–malate cycle (Fig. 1). In contrast, glucose was not necessary for the insulin-stimulated increase in TCA cycle metabolites, with nonglucose sources being utilized in the absence of glucose (Fig. 1). Our previous work showed that glucose was also not required for insulin to stimulate respiration, which we proposed was due to a rising energy demand in response to insulin action (16). These findings concur with our previous observations whereby glycolytic metabolites increased with insulin stimulation at a similar speed to glucose uptake, with differing kinetics to TCA cycle metabolites (7, 9). We speculate that this segregation exists to enable respiration to support energy production, whereas glycolysis and other glucose-dependent pathways meet the other demands for insulin-stimulated anabolism, such as carbon and reducing power.

We demonstrated here that glucose metabolism is not only sufficient, but necessary, for insulin-stimulated lipid anabolism. First, insulin-responsive *de novo* lipogenesis and accumulation of malonyl-CoA were glucose-dependent, whereas basal lipogenesis was unaffected (Fig. 1*E* and 2). This suggests that the insulin-stimulated portion of newly synthesized fatty acids is likely glucose-derived. Conversely, the basal lipogenesis from nonglucose sources would explain why insulin had a much greater effect (fold change) on glucose incorporation into fatty acid compared with total fatty acid synthesis (Fig. 2*D*); this contrasts with studies using minimal medium, in which these rates responded with similar fold changes to insulin (23). This implies that the nutritional milieu influences the effect of insulin on global lipogenesis. Second, glucose-dependent pathways included the pyruvate–malate cycle and pentose phosphate pathway (Fig. 1). We previously found both to closely interact with glycolysis in adipocytes (7). Both are responsible for generating NADPH, with the former being particularly prominent in cultured adipocytes and rodent adipose tissue (21, 40). Our data suggest that in adipocytes, these NADPH sources are sensitive to exogenous glucose availability. Third, G3P, derived from glycolysis, accumulated in a glucose-dependent manner (Fig. 1). Furthermore, exogenous glucose was substantially incorporated into the glycerol backbone of glycerolipids from both our radiotracer and ^{13}C-lipidomics data (Fig. 2). This concurs with previous observations that glucose supports fatty acid esterification in primary adipose explants from rodents (11). Conversely, we found G3P to be an important carbon sink for glucose metabolism (22), highlighting its priority as a metabolic end point in adipocytes. Indeed, G3P abundance was more sensitive to insulin than glyceride–glycerol synthesis (Figs. 1*E* and 2*A*), indicating an accumulation of this intermediate faster than its incorporation into glycerolipid under our experimental conditions. This likely enables the adipocyte to store exogenous fatty acids as triglyceride. Fourth, glucose suppressed lipogenesis from leucine (Fig. 3). BCAAs serve as lipogenic substrates in cultured adipocytes and adipose tissue (12–15). Our data

Figure 4. Glucose suppresses fatty acid oxidation, but not lipolysis. *A*, schematic depicting the hormonal control of lipolysis by insulin (*Ins*) or CL 316,243 (*CL*) and subsequent mobilization of lipid stores. Other abbreviations defined at the end. *B*, 3T3-L1 adipocytes were treated with or without 100 nM insulin for 1 h in KRP buffer, supplemented with BSA-conjugated palmitate to achieve a final concentration of 0.25% (w/v) BSA, 125 μM palmitate, and 2 μCi/ml [1-^{14}C] palmitate. This assay buffer was supplemented further with either no sugar (*None*) or 25 mM sugar (glucose, *Glc*; galactose, *Gal*). Incorporation of fatty acid into CO_2 (fatty acid oxidation) was measured as described under "Experimental procedures." The data are presented as means ± S.E. (*error bars*) from four separate experiments. *C*, 3T3-L1 adipocytes were treated with 100 nM insulin and/or 1 nM CL for 1 h in KRP buffer, supplemented with 3.5% (w/v) fatty acid–free BSA and 25 mM sugar (glucose or galactose). Following treatment, the cells were harvested, and lysates were subjected to Western blotting. The blots shown are representative of three separate experiments. Nonspecific bands denoted by *asterisks*. Quantification is shown in Fig. S4 (*A* and *B*). *D* and *E*, 3T3-L1 adipocytes were treated as described in *C*, with either no sugar (*None*) or 25 mM sugar (glucose or galactose). Following treatment, the rate of lipolysis was assessed by the release of glycerol (*D*) or free fatty acids (*E*), as described under "Experimental procedures." The rate of anti-lipolysis (*right panel*) was determined by comparing the Ins-CL condition to the CL condition for each sugar, *i.e.* anti-lipolysis (%) = 100 × (1 – Ins-CL rate/CL rate). The data are presented as means ± S.E. (*error bars*) from four separate experiments. *, $p < 0.05$; *ns*, $p > 0.05$ (not significant), by two-sample *t* test. *F*, 3T3-L1 adipocytes were treated for 1 h with 100 nM insulin and/or triacsin C (*Tc*) in KRP buffer, supplemented with BSA-conjugated palmitate as described in *B* and 25 mM glucose. Following treatment, the lipids were extracted, resolved by TLC, and subjected to phosphorimaging. The phosphorimaging result shown is representative of two separate experiments. Quantification is shown in Fig. S4*C*. *G*, 3T3-L1 adipocytes were treated for 1 h with Tc in KRP buffer, supplemented with BSA-conjugated palmitate as described in *B*. Fatty acid oxidation was measured as described under "Experimental procedures." The data are presented as means ± S.E. (*error bars*) from four separate experiments. *H*, 3T3-L1 adipocytes were treated as described in *C*, with 25 mM sugar (glucose or galactose) with or without 20 μM Tc. Following treatment, the rate of lipolysis was assessed by the release of free fatty acids, as described under "Experimental procedures." The rate of anti-lipolysis (*right panel*) was calculated as described for *D* and *E*. The data are presented as means ± S.E. (*error bars*) from four separate experiments. *, $p < 0.05$; *ns*, $p > 0.05$ (not significant), by two-sample *t* test. *CE*, cholesterol ester; *DAG*, diacylglyceride; *FA*, fatty acid(s); *FAO*, fatty acid oxidation.

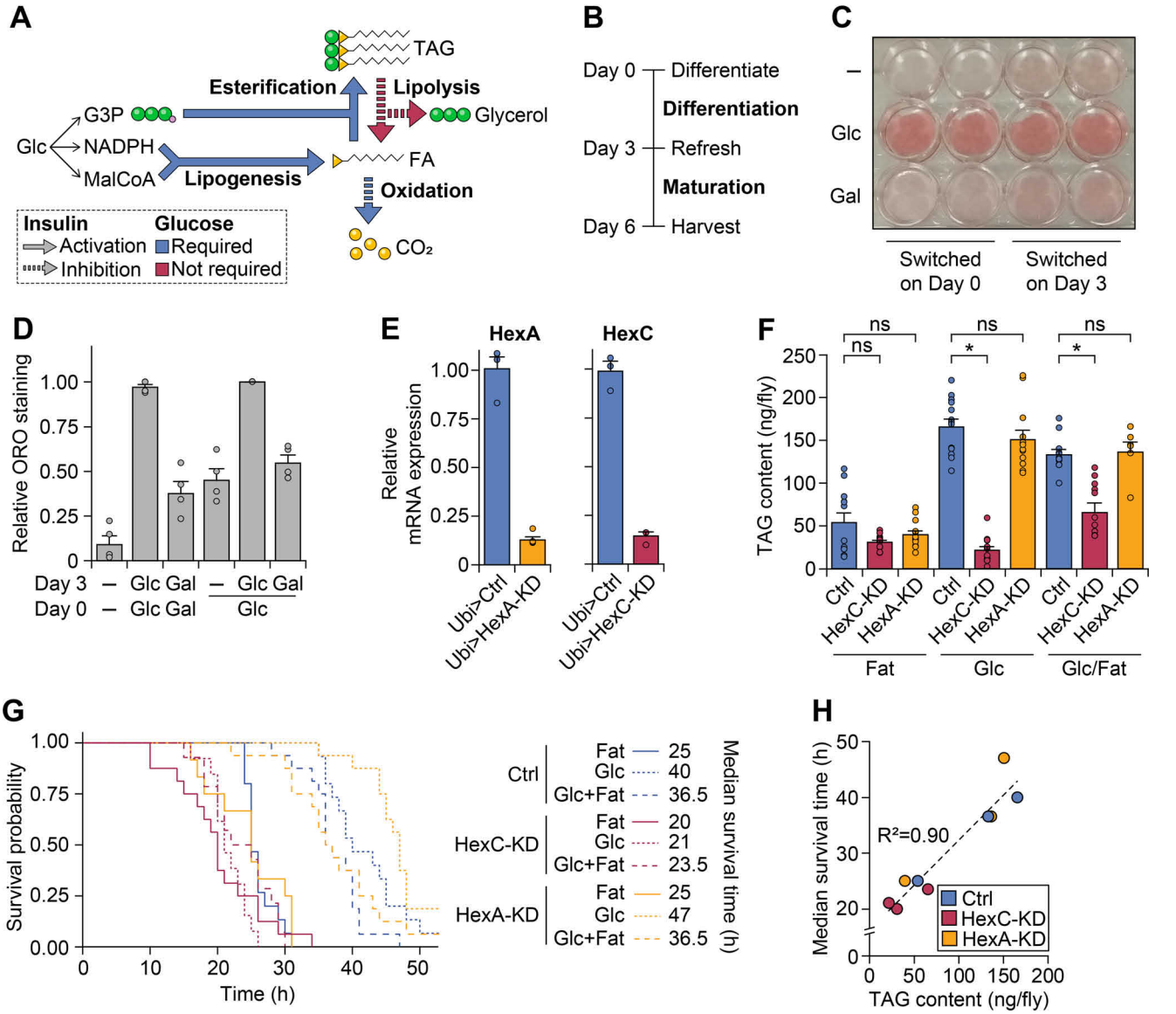

Figure 5. Lipid storage is sensitive to glucose metabolism. *A*, schematic summarizing how insulin and glucose (*Glc*) influence lipid metabolism, based on the data from Figs. 1–4. *B*, schematic depicting the timeline of adipogenesis for 3T3-L1 preadipocytes. The details are provided under "Experimental procedures." *C* and *D*, 3T3-L1 preadipocytes were differentiated in BSF-DMEM supplemented with 10% (v/v) fetal bovine serum and 2 mM GlutaMAX, and either no sugar (–) or 25 mM sugar (glucose, *Glc* or galactose, *Gal*). The cells were differentiated in the presence of glucose by default. The sugar was switched either on day 0, whereby that same sugar was maintained during differentiation and maturation, or on day 3, whereby glucose was present during differentiation and the sugar type was manipulated only at the maturation stage. Following maturation, the cells were stained for lipid content using Oil Red O (*ORO*) staining. A representative photograph is shown in *C*, with quantification for relative ORO staining presented as means ± S.E. (*error bars*) in *D* from four separate experiments. *E*, *Drosophila* male flies expressing either whole-body control (*ubi*-GAL4 > UAS-CG-none, *Ubi* > *Ctrl*), HexA-specific (*ubi*-GAL4 > UAS-*HexA*^{GD9964}, *Ubi* > HexA-KD), or HexC-specific (*ubi*-GAL4 > UAS-*HexC*^{GD12378}, *Ubi* > HexC-KD) knockdown were harvested for RNA. *HexA* (*left panel*) or *HexC* (*right panel*) RNA expression levels were quantified. The data are presented as means ± S.E. (*error bars*) from three biological replicates per condition. *F*, *Drosophila* male flies expressing fat body-specific control (*cg*-GAL4 > UAS-CGnone, *Ctrl*), HexA-specific (*cg*-GAL4 > UAS-*HexA*^{GD9964}, HexA-KD), or HexC-specific (*cg*-GAL4 > UAS-*HexC*^{GD12378}, HexC-KD) knockdown were fed for 10 days with diets supplemented with fat and/or glucose, as detailed under "Experimental procedures." Following this feeding regime, the flies were assayed for lipid content by $CHCl_3$-MeOH extraction and measurement by a triglyceride assay. The data are presented as means ± S.E. (*error bars*) from 10 to 12 biological replicates pooled from two separate experiments (except HexA-KD-Glc/Fat, which was 6 biological replicates from 1 experiment). *, $p < 0.05$; *ns*, $p > 0.05$ (not significant), by two-sample *t* test. *G*, *Drosophila* male flies were bred and exposed to diets as described for *F*. Following this feeding regime, survival upon starvation was assessed by automated monitoring. Activity was monitored as beam crosses at 5-min intervals, as described under "Experimental procedures." The data are from 16 individual flies per diet. The median survival time is also presented (*right panel*). A Cox proportional hazards regression analysis demonstrated a significantly poorer survival prognosis in HexC-KD animals compared with control animals and diets supplemented with fat compared with glucose alone ($p < 0.01$ for both). *H*, median survival times (from *G*) were plotted against mean lipid content (from *F*) for each diet/genotype condition.

showed that leucine could be incorporated into lipid in an insulin-dependent manner, but this was abolished in the presence of glucose (Fig. 3). This suggests that in the absence of glucose, insulin diverts additional leucine for lipogenesis, but the use of alternative substrates cannot support the same level of insulin-stimulated lipogenesis observed when glucose is available (Fig. 2). Although 25 mM glucose was used in these experiments (Fig. 3), given that glucose incorporation into lipid does not change markedly between 5 and 25 mM glucose in the medium (Fig. S2*B*), we anticipate that this phenomenon would similarly

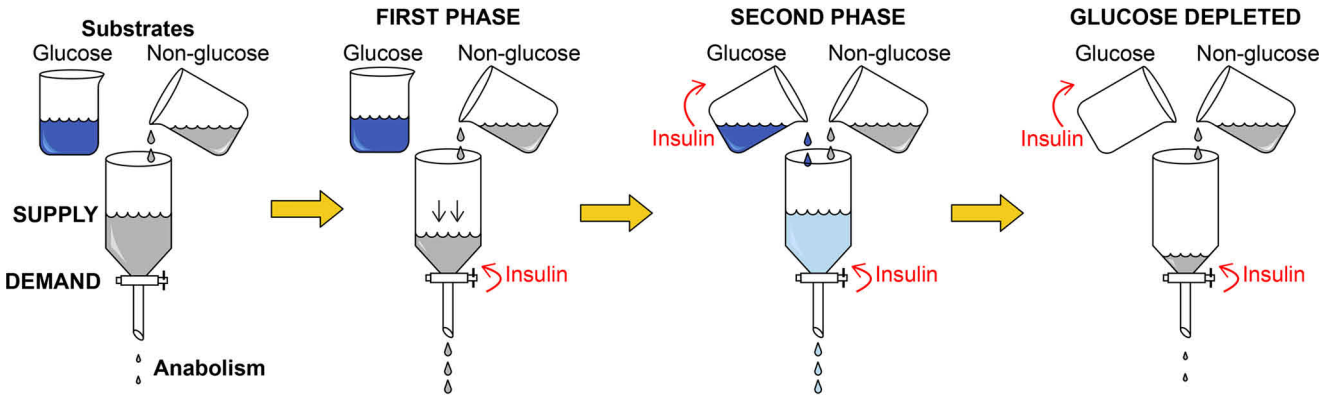

Figure 6. Proposed relationship between insulin, glucose, and adipose anabolism. Glucose and other carbon sources (*e.g.* BCAAs) provide the supply to meet an adipocyte's anabolic demands (*e.g.* lipid synthesis). Insulin utilizes kinase signaling cascades to activate anabolic enzymes and promote the translocation of glucose transporter GLUT4 to the plasma membrane. Because of the lag in GLUT4 translocation, this results in anabolism being stimulated before substantial glucose uptake occurs (9), resulting in two phases of insulin action: first, the activation of anabolism by kinase signaling independently of glucose, and second, glucose is taken up and metabolized to meet the increase in anabolic demand. If glucose is absent or becomes depleted, this anabolic demand cannot be met with other carbon sources, leading to the depletion of anabolic substrates and curbing of adipose anabolism. Further details appear under "Discussion."

occur at physiological glucose concentrations. Lastly, glucose was required for insulin-dependent suppression of fatty acid oxidation (Fig. 4), as observed previously in rodent primary adipose explants (11). This is likely due to inhibition of fatty acid import into the mitochondria by malonyl-CoA (25, 41), which increased with insulin treatment in a glucose-dependent manner (Fig. 1). Overall, this demonstrates that even in the presence of other lipogenic substrates, glucose is necessary to provide the substrates, cofactors, and metabolic control required for insulin to stimulate lipid anabolism (and curb oxidation) in adipocytes.

Our work also demonstrated instances in which signal transduction acted independently of glucose to mediate specific actions of insulin, suggesting that there are different phases to insulin action. For instance, insulin could suppress lipolysis without glucose present (Fig. 4). Indeed, insulin stimulation rapidly abolishes protein A kinase activity, enabling lipolysis to be suppressed before glucose uptake is maximized (9, 42). Furthermore, glucose metabolism had no direct impact on acute, insulin-stimulated kinase signaling (Figs. 3*F* and 4*C*), as we have observed previously when compared with galactose (16) or no sugar (data not shown). Together, this suggests that insulin acts in two phases (Fig. 6). The first phase is glucose-independent, whereby insulin initially turns off lipolysis and stimulates anabolism by phosphorylation of metabolic proteins (9). Anabolism heightens energy demands, which increases respiration (16). Respiration is not dependent on glucose (16) and thus is able to meet these energy demands independent of nutrient availability. In the second phase, glucose is taken up and metabolized, providing the carbon, NADPH, and G3P required to sustain insulin-stimulated lipid synthesis and storage. If glucose is absent (or glucose uptake is inadequate), these precursors cannot be provided sufficiently from other sources and are thus depleted upon insulin stimulation, ultimately curbing lipid anabolism (Fig. 6). Thus, insulin facilitates the temporal separation of demand and supply, making lipid metabolism ultimately dependent on glucose metabolism.

Consequently, we found that lipid levels were sensitive to glucose availability. We showed that glucose was required for lipid accumulation during adipocyte differentiation (Fig. 5). This concurs with other studies that have demonstrated that glucose is required for differentiation (27, 28, 43), both for expression of adipocyte-specific proteins and lipid accumulation. Unlike these previous studies, however, we specifically modulated glucose availability during the maturation stage of differentiation, to minimize the impact of glucose on lipogenic gene expression during the early stages of differentiation. We complemented these experiments by considering whole-body lipid storage and starvation resistance in *Drosophila* (Fig. 5). The fly fat body functions as a combination of liver and adipose tissue. Because both are lipogenic tissues, interrogating the metabolism of flies with fat body-specific gene knockdowns provided a first step to assessing glucose's role in lipid storage. Our data demonstrated that both dietary glucose and glucose metabolism specifically in the fat body were required to maximize lipid storage (Fig. 5). In the future, the effect of adipose glucose metabolism on lipid storage should be tested in mammals that have distinct adipose and liver tissues. For instance, male adipose-specific GLUT4-knockout mice had unaffected lipid storage based on adipose tissue measurements, blood nonesterified fatty acids (NEFAs), and ectopic lipid content (6). However, to our knowledge, these mice were not challenged by a high-fat, high-sucrose diet, which would test lipid storage under conditions of insulin resistance.

Overall, these data highlight the importance of glucose metabolism to support insulin-stimulated lipid storage, providing a complementary regulatory mechanism to kinase signaling. This has implications for insulin resistance, for which in adipose tissue the insulin-dependent regulation of glucose uptake is impaired, but anti-lipolysis remains intact (17). This would have flow-on effects for the remainder of lipid metabolism, placing adipose glucose metabolism as an intermediate rather than an end point of insulin resistance. We anticipate that impaired adipose glucose metabolism would ultimately diminish lipid storage capacity in adipose tissue, potentially

contributing to ectopic lipid storage and ultimately whole-body insulin resistance (reviewed in Ref. 44).

Experimental procedures

Reagents

The following pharmacological agents were used in this study: insulin (Sigma–Aldrich catalog no. I5500), CL 316,243 (Sigma–Aldrich catalog no. C5976), and triacsin C (Sigma–Aldrich catalog no. T4540). The following substrate tracers were used in this study: [U-^{13}C]glucose (Omicron Biochemicals catalog no. GLC-082), [U-^{13}C]galactose (Omicron Biochemicals catalog no. GAL-013), [U-^{14}C]glucose (PerkinElmer catalog no. NEC042X001MC), L-[U-^{14}C]leucine (PerkinElmer catalog no. NEC279E050UC), [1-^{14}C]palmitic acid (PerkinElmer catalog no. NEC075H001MC), and [^{3}H]H_2O (PerkinElmer catalog no. NET001B000MC).

Cell culture

3T3-L1 fibroblasts were maintained and differentiated into adipocytes as described previously (9, 45), using medium A, consisting of bicarbonate-buffered DMEM (Life Technologies, catalog no. 11960), supplemented with 10% (v/v) fetal bovine serum (Life Technologies, catalog no. 16000044) and 2 mM GlutaMAX (Life Technologies, catalog no. 35050061). Unless otherwise specified, the adipocytes were used between days 9 and 12 after the initiation of differentiation. At least 90% of the cells were differentiated prior to experiments. These cells were routinely tested for mycoplasma infection.

Unless otherwise specified, prior to insulin stimulation treatments, the cells were serum-starved for at least 2 h. This involved washing cells three times with PBS and incubating them in basal medium. By default, the basal medium was medium B, which consisted of bicarbonate-buffered DMEM (Life Technologies catalog no. 11960), supplemented with 0.2% (w/v) bovine serum albumin (BSA, Bovostar) and 2 mM GlutaMAX.

For metabolic assays within the CO_2 incubator, the cells were washed after serum starvation: once with PBS and then with bicarbonate-buffered, substrate-free DMEM (BSF-DMEM), which consisted of substrate-free DMEM (Sigma-Aldrich catalog no. D5030), supplemented with 44 mM $NaHCO_3$ and adjusted to pH 7.4 with CO_2 (dry ice). The cells were then incubated in medium BS, which consisted of BSF-DMEM, supplemented with 0.2% (w/v) BSA, 1 mM GlutaMAX, 1 mM glutamine, and sugar (glucose/galactose) as specified in the figure legends. Glutamine was supplemented in addition to GlutaMAX to provide an immediate source of glutamine substrate for short-term experiments. The experiments were performed at 37 °C with 10% CO_2.

For metabolic assays performed outside of the CO_2 incubator, the cells were treated in either DMEM or KRP buffer, both buffered at pH 7.4 with 30 mM Na-HEPES and 1 mM $NaHCO_3$ (16, 22, 46). For experiments with DMEM, the cells were washed once with PBS and then with HEPES-buffered, substrate-free DMEM (HSF-DMEM), which consisted of substrate-free DMEM (Sigma–Aldrich catalog no. D5030) supplemented with 30 mM Na-HEPES (pH 7.4) and adjusted to pH 7.4 with NaOH. The cells were then incubated in medium C, which consisted of HSF-DMEM, supplemented with 0.2% (w/v) BSA, 1 mM $NaHCO_3$ (added fresh), 1 mM glutamine, 1 mM GlutaMAX, and sugars (glucose/galactose) as specified in the figure legends, with pH adjusted to 7.4. Alternatively, for experiments with KRP buffer, the cells were washed thrice with PBS before incubation in KRP buffer. The KRP buffer was as described previously (47), except with a modified pH buffer system: 0.6 mM Na_2HPO_4, 0.4 mM NaH_2PO_4, 120 mM NaCl, 6 mM KCl, 1 mM $CaCl_2$, 1.2 mM $MgSO_4$, 30 mM Na-HEPES (pH 7.4), and 1 mM $NaHCO_3$ (added fresh), with pH adjusted to 7.4. The KRP was also supplemented with BSA and substrates (palmitate, glucose or galactose), as described in the figure legends and specific assays below. Palmitate was conjugated to fatty acid–free BSA (Sigma–Aldrich catalog no. A7030) prior to treatment (48). Following the addition of assay medium and drug treatments, the plates were sealed with TopSeal-A PLUS (PerkinElmer) and incubated in a 37 °C incubator.

Quantification of intracellular metabolites by targeted metabolomics

Following treatment, the cells washed twice with cold 5% (w/v) mannitol on ice and harvested for intracellular metabolites, which were analyzed by capillary electrophoresis- and ion chromatography–coupled mass spectrometry as described previously (9). Data analysis, including natural abundance correction and derivation of ^{13}C-labeled abundance, was performed as described previously (9, 22). Principal component analysis was performed as described previously (9).

Tracer lipidomics

Following treatment, an aliquot of medium was removed, and the cells were then washed thrice with cold PBS on ice, scraped in 400 μl of PBS, and frozen. The cell lysates were extracted for lipid using a single-phase chloroform/methanol protocol as previously described (49). Lipid extracts were run on a Thermo Scientific Q Exactive HF-X hybrid quadrupole-Orbitrap mass spectrometer (Thermo Fisher Scientific) in conjunction with a Thermo Vanquish HPLC unit (Thermo Fisher Scientific). The mass spectrometer was run in full mass spectrometry (MS) mode at a resolution of 240,000. A ZORBAX Eclipse Plus C18 column (2.1 × 100 mm, 1.8 μM, Agilent) was used at 45 °C at a flowrate of 400 μl/min with the following running conditions: solvent A, 50% H_2O, 30% acetonitrile, 20% isopropanol (v/v/v) containing 10 mM ammonium formate; and solvent B, 1% H_2O, 9% acetonitrile, 90% isopropanol (v/v/v) containing 10 mM ammonium formate. Starting at 15% solvent B, this was increased to 50% B over 2.5 min and ramped to 56% B over 0.1 min. At 2.6–9 min, the solvent B% was increased to 70% B, with a rapid increase at 9–9.1 min to 80% B. Between 9.1 and 29 min, solvent B was increased from 80% B to 100% B. The column was then reduced back to 15% B and equilibrated until the 35-min mark. Species of interest were identified using a combination of retention time and exact mass. Both the monoisotopic species and their labeled isotopes were integrated using R (3.6.1) using their respective exact masses. The ^{13}C enrichment of the carbon backbones for each lipid species was calculated from extracted mass isotopologues, by using in-house

MATLAB optimization scripts to correct for naturally occurring isotopes in each species, based on their respective parent ion molecular formula and the length of carbon backbone (50).

Lipid synthesis assay

Following incubation with [^{3}H]H_2O or [U-^{14}C]glucose in 12-well culture plates, the cells were washed thrice with cold PBS on ice and quenched by freezing the plates at −80 °C. The cells were processed as described previously (7, 22), with minor modifications. The cells were scraped in 1.1 ml of 0.6% (w/v) NaCl on ice. A 100-μl aliquot was taken; to this aliquot, 0.1 volume of 10% (w/v) SDS was added, and the mixture was quantified for protein content using the Pierce bicinchoninic acid assay kit (Thermo Fisher Scientific), according to the manufacturer's instructions. The remainder (1 ml) was extracted for lipids by MeOH-$CHCl_3$ extraction, whereby 4 ml of 2:1 (v/v) mixture of $CHCl_3$/MeOH was added prior to extraction. An aliquot of the organic phase was evaporated to dryness under N_2 gas and resuspended in Ultima Gold XR scintillation fluid (PerkinElmer) and subjected to liquid scintillation counting using the Tri-Carb 2810 TR β-counter (PerkinElmer). Radiation counts were adjusted to cell-free controls, aliquots of NaCl solution that were extracted in parallel to the cell lysates. This determined the incorporation of radiotracer into the total lipid pool.

A second aliquot of the organic phase was evaporated to dryness, and saponifiable lipids were isolated as described previously (7, 22). Briefly, the sample was saponified using ethanolic KOH, acidified by H_2SO_4, isolated by petroleum ether extraction, and evaporated to dryness under N_2 gas, and radioactivity was assayed as described above. This determined the incorporation of radiotracer into the saponifiable lipid pool. The difference between total and saponifiable lipid pools determined the nonsaponifiable lipid pool.

The rate of synthesis of fatty acids and glyceride–glycerol were derived from the radiotracer incorporated into the saponifiable and nonsaponifiable lipid pools, respectively. It was assumed that C16 fatty acid was the predominant fatty acid synthesized (23, 24, 51). The [^{3}H]H_2O tracer was used to derive the total rate of newly synthesized lipid, calculated based on the estimate that 13.3-μg atoms of hydrogen are incorporated into 1 μmol of synthesized C16 fatty acid (23, 24) and 3.3-μg atoms of hydrogen are incorporated into 1 μmol of glyceride–glycerol (23). The [U-^{14}C]glucose tracer was used to derive the rate of newly synthesized lipid from glucose, calculated based on the assumption that 1 mol of glucose generates 6/16 (0.375) mol of C16 fatty acid or 6/3 (2) mol of glyceride–glycerol.

Substrate oxidation assay

Following the addition of medium, radiotracer label, and drug treatments, substrate oxidation was assessed as described previously (22, 48). Briefly, this involved installing a gas trap in each well, sealing the culture plate, incubating at 37 °C for the duration of the experiment, and quenching cells by acidification. Incorporation of radiotracer into the gas-trapping solution was measured by liquid scintillation counting, with radiation counts adjusted to cell-free controls.

Protein synthesis assay

To measure the incorporation of substrate into newly synthesized protein, we made several modifications upon our previously published protein synthesis assay (17, 52). First, we used medium C instead of leucine-free DMEM to keep the medium consistent with other experiments in this study. Second, we used ^{14}C-labeled leucine instead of ^{3}H-labeled leucine to maintain consistency with other experiments in this study that followed the fate of leucine carbon (*e.g.* incorporation into CO_2 and lipid). Finally, instead of trichloroacetic acid, we isolated protein by precipitation with acetone, a reagent routinely used in proteomics workflows, because this generated a better signal (Fig. S3, *A* and *B*).

Cell culture treatments were performed as described above, with the addition of parallel cultures being treated with 5 μM cycloheximide during the last 30 min of the serum-starvation period and throughout the treatment/labeling period. Following treatment, the cells were washed thrice with cold PBS on ice and scraped in cold PBS (200 μl/well for 12-well culture plates). Four volumes (800 μl) of cold acetone was added, and the samples were mixed before incubation at −30 °C for at least 2 h. Protein precipitates were pelleted by centrifugation for 20 min at 16,000 × *g* and 4 °C. Each pellet was washed by resuspension in 1.3 ml of cold 80% (v/v) acetone, using a cold sonicating water bath. The samples were incubated again at −30 °C for at least 2 h and centrifuged for 20 min at 16,000 × *g* and 4 °C. Each protein pellet was solubilized with 500 μl of buffer consisting of 50 mM NaOH and 1% (v/v) Triton X-100, using the ThermoMixer C (Eppendorf) for 30 min at 65 °C, with shaking at 1000 rpm.

Incorporation of radiotracer into the protein fraction was measured by liquid scintillation counting and normalized to protein content, which was determined using the Pierce bicinchoninic acid assay kit (Thermo Fisher Scientific) according to the manufacturer's instructions. For each condition, the difference in (radiotracer) substrate incorporation with *versus* without cycloheximide cotreatment determined the incorporation of substrate into newly synthesized protein.

Thin layer chromatography (TLC)

Following treatment, the cells were washed thrice with cold PBS on ice, and lipids were isolated by MeOH-$CHCl_3$ extraction as described above for the lipid synthesis assay. Lipid extracts were evaporated to dryness under N_2 gas and resuspended in a small volume (50 μl) of $CHCl_3$ prior to resolution by TLC. TLC glass plates with silica gel 60 (20 × 20 cm, Merck–Millipore catalog no. 1057210001) were baked at 100 °C for 1 h and washed by being subjected to a solvent system consisting of a 70:30 (v/v) mixture of $CHCl_3$/MeOH.

The TLC plate was baked again at 100 °C for 1 h before samples and natural ("cold") standards were loaded in 1.5-cm lanes; standards included cholesteryl oleate (representative cholesterol ester; Sigma–Aldrich catalog no. C9253), glyceryl tripalmitin (representative TAG; Sigma–Aldrich catalog no. T5888), dipalmitin (~50:50 mixture of 1,2- and 1,3-diacylglyceride; Sigma–Aldrich catalog no. D2636), and palmitic acid (representative fatty acid, Sigma–Aldrich catalog no. P5585). The

TLC plate was then subjected to a resolving solvent system for neutral lipids, consisting of an 80:20:1 (v/v/v) mixture of hexane/diethylether/acetic acid (53). Once dried, a ^{14}C-labeled solution of known radioactivity (*e.g.* KRP containing BSA-conjugated palmitate with [1-^{14}C]palmitate radiotracer) was applied to several places on the TLC plate: (i) at the origin and solvent front of resolving solvent system, in the margin outside the lanes, to identify bands on the phosphorimage using R_f values; and (ii) at a standard curve between the solvent front and the top of the plate, to convert phosphorimaging band intensity into radioactivity (radiotracer incorporation). The TLC plate was baked at 70 °C for 30 min before visualization by phosphorimaging with the Typhoon FLA 9500 (GE Healthcare). Standards were identified by staining the TLC plate with 0.02% (w/v) 2′,7′-dichlorofluorescein in ethanol (Sigma–Aldrich catalog no. D6665) and visualization under long-wave UV light.

Lipid bands of interest on the phosphorimage were identified by the migration of cold standards and quantified using the ^{14}C standard curve. Image analysis was performed using Fiji software (54).

Western blotting

Following treatment, the cells were washed thrice with cold PBS on ice and harvested for protein, and the lysates were subjected to Western blotting as described previously (22). Antibodies detecting pS473-Akt (clone 587F11, catalog no. 4051), pT308-Akt (clone D25E6, catalog no. 13038), Akt (clone 11E7, catalog no. 4685), pT246-PRAS40 (clone C77D7, catalog no. 2997), pS235/6-S6 (clone D57.2.2E, catalog no. 4858), pT389-p70 S6K (catalog no. 9205), p70 S6K (clone 49D7, catalog no. 2708), and pS660-HSL (catalog no. 4126) were obtained from Cell Signaling Technology. The antibody detecting pS522-PLIN1 (catalog no. 4856) was obtained from Vala Sciences. The antibody detecting PKA IIα-reg (catalog no. sc-136262) was obtained from Santa Cruz Biotechnology. The antibody detecting α-tubulin (clone DM1A, catalog no. T9026) was obtained from Sigma–Aldrich. Densitometric analysis was performed either using Fiji software (54) or LI-COR Image Studio (LI-COR Biosciences).

Lactate production assays

Following treatment, lactate content of the conditioned medium was measured either enzymatically using the hydrazine sink method (for total lactate abundance only) or by targeted liquid chromatography coupled-MS (for abundance of lactate isotopologues), both as described previously (22, 55).

Lipolysis assays

Following treatment in 24-well culture plates, conditioned medium was centrifuged for 10 min at 2000 × *g* and 4 °C to remove cellular debris. One aliquot of supernatant was assayed for glycerol content using a colorimetric glycerol assay kit (Sigma–Aldrich, catalog no. FG0100), according to the manufacturer's instructions. Glycerol levels were quantified using a standard curve of glycerol (Sigma–Aldrich catalog no. G7793), added to naïve culture medium.

To measure free fatty acid levels, a second aliquot of supernatant was extracted using MeOH-$CHCl_3$ to isolate free lipids and concentrate lipid content. Glass tubes were used during this extraction to avoid contaminants leached from plastic tubes by $CHCl_3$, which we found interfered with the NEFA assay (data not shown). The sample (200 μl) was transferred to a borosilicate glass tube (Kimble Chase, catalog no. 60B12B), and four volumes (800 μl) of a 2:1 (v/v) mixture of $CHCl_3$:MeOH was added. The mixture was gently vortexed for 10 s and centrifuged for 10 min at 1600 × *g* and 4 °C. 400 μl of the lower (organic) phase was transferred to a fresh glass tube and evaporated to dryness under N_2 gas. Dried lipids were solubilized in 500 μl of warm EtOH (preheated to 37 °C, to aid solubilization), transferred to plastic 1.5-ml microcentrifuge tubes, and lyophilized using an EZ-2 centrifugal evaporator (GeneVac). This transfer step was performed to permit resolubilization in a smaller volume (in the next step), and the use of EtOH in these tubes did not generate contaminants that substantially interfered with the NEFA assay (data not shown). Consequently, dried lipids were finally solubilized in 50 μl of EtOH, using the ThermoMixer C (Eppendorf) for 10 min at 37 °C, with shaking at 1000 rpm. The samples were pulse-spun by microcentrifuge and assayed for fatty acid content using a colorimetric NEFA assay kit (WAKO, catalog no. 294-63601), according to the manufacturer's instructions. Fatty acid levels were quantified using a standard curve of oleic acid (standard provided in the kit), added to EtOH. Extraction efficiency was assessed by control samples, prepared by diluting palmitate–BSA conjugate in naïve medium, which were then extracted and assayed in parallel to the samples.

Glycerol release and free fatty acid release in the medium were normalized to cellular protein content. The latter was determined following removal of medium, whereby cells were washed thrice with cold PBS on ice and lysed in PBS containing 1% (v/v) Triton X-100. Protein quantification was performed using the Pierce bicinchoninic acid assay kit (Thermo Fisher Scientific), according to the manufacturer's instructions.

Oil red O staining assay

Oil red O (ORO) stock solution was prepared as a 0.35% (w/v) mixture of Oil Red O (Sigma–Aldrich catalog no. O-0625) in isopropanol, which was stirred overnight, and filtered with a 0.2-μm filter. From this, an ORO working solution was prepared as a 60:40 (v/v) mixture of ORO stock solution and water, which was filtered with a 0.2-μm filter immediately prior to use.

Following treatment, the cells were washed thrice with cold PBS on ice and fixed with 3.7% (w/v) paraformaldehyde in PBS for at least 30 min. The fixing solution was aspirated, and the cells were washed twice with 60% (v/v) isopropanol. The wells were dried completely before staining for 10 min with ORO working solution (0.5 ml/well). Wells were then washed thoroughly with water and dried completely. Bound ORO was eluted using 0.6 ml of (100%) isopropanol, with gentle rocking on an orbital shaker for 10 min. The elution step was repeated, and the eluates were combined (1.2 ml total). ORO staining was quantified by measuring the absorbance of the eluate at 500

nm, using the Infinite M1000 Pro (Tecan). To account for non-specific staining (*e.g.* ORO binding the plastic wells), the absorbances were adjusted to cell-free wells that were fixed, stained, and eluted in parallel to the treatment wells.

To account for differences in cell number, crystal violet staining was performed as described previously (56), with minor modifications. The wells were washed twice with isopropanol to remove residual ORO, dried completely, and stained with a 1% (w/v) aqueous solution of crystal violet (Sigma–Aldrich catalog no. V5265) for 10 min (0.5 ml/well). The wells were then washed thoroughly with water and dried completely before bound crystal violet stain was eluted twice with 0.6 ml of MeOH per elution (1.2 ml total) and gentle rocking on an orbital shaker for 10 min for each elution. Crystal violet staining was quantified by measuring the absorbance of the eluate at 570 nm, using the Infinite M1000 Pro (Tecan). As with the ORO staining, the absorbances here were adjusted to cell-free wells.

To obtain "relative ORO staining," the adjusted ORO absorbances were made relative to the control condition, and likewise for crystal violet absorbances. Finally, for each condition, the relative ORO absorbance was normalized to the relative crystal violet absorbance, resulting in a quantification of ORO staining that was normalized to cell number.

Methodology for Drosophila experiments

Fly stocks, maintenance, and crosses—Fly strains used in this study included *CG*-none RNAi GD12145 (Vienna *Drosophila* Resource Center) and *HexC* RNAi GD12378 (catalog no. 35337, Vienna *Drosophila* Resource Center), *HexA* RNAi GD9964 (catalog no. 21054, Vienna *Drosophila* Resource Center), *ubiquitous*-GAL4/Cyo (catalog no. 32551, Bloomington), and *CG*-Gal4 (catalog no. 7011 Bloomington). The flies were maintained as described previously (22). To generate fat body–specific knockdown flies, 20 *CG*-Gal4 females were crossed with 5 *CG*-none (control), *HexC* RNAi, or *HexA* RNAi male flies. For whole-body knockdown flies, *ubiquitous*-GAL4 females were used instead.

Quantification of RNA expression—RNA isolation and quantitative real-time PCR were performed as described previously (22). Each biological replicate consisted of 10 flies. *Tubulin* was used as a housekeeping gene (22), and the following primers were used to amplify target genes: *HexA* (forward, 5′-CTGCTTCTAACGGACGAACAG-3′; reverse, 5′-GCCTTGGGATGTGTATCCTTGG-3′) and *HexC* (forward, 5′-CCCGGTGTGGACCTATTCG-3′; and reverse, 5′-GTGGCAGATATGCGGTCTTCA-3′). Relative gene expression was calculated using the $\Delta\Delta C_t$ method.

Experimental diets—Diets contained 5% (w/v) yeast (Baker's Yeast, Lowen) and 1% (w/v) agar (Sigma–Aldrich catalog no. A1296), supplemented with 20% (w/v) glucose (Sigma–Aldrich catalog no. G8270) and/or 10% (w/v) lard (York Foods). In 100 ml of diet mixture, supplemented glucose would provide 314 kJ (assuming 15.7 kJ/g glucose), and lard would provide 370 kJ (based on 3700 kJ/100 g, from manufacturer's product information).

From the RNAi crosses, 3–5-day-old male progeny were placed on each diet for 10 days, with the food changed every second day. Following this feeding regime, the flies were either processed for lipid content or starvation resistance, as described below.

Triglyceride assay—Each biological replicate consisted of six flies. To assess lipid content, the flies were quenched and washed with increasingly diluted solutions of isopropanol, as described previously (22), to remove excess food. The flies were then extracted for lipid by MeOH-$CHCl_3$ extraction, as described previously (22). Lipid extracts were evaporated to dryness under N_2 gas and reconstituted with EtOH. The samples were pulse-spun by microcentrifuge and assayed for lipid content by a colorimetric triglyceride assay (Thermo Fisher Scientific catalog no. TR22421), according to the manufacturer's instructions. Precimat glycerol reagent (Thermo Fisher Scientific catalog no. NC0091901; Roche Diagnostics catalog no. 10166588130) was used as a reference standard.

Starvation resistance assay—Starvation resistance was measured using the *Drosophila* Activity Monitoring 2 (*DAM2*) system (Trikinetics Inc.). 16 flies were used for each condition. The flies were loaded into DAM2 tubes containing 2% (w/v) agar and monitored every 5 min for fly movement. The flies were considered deceased when no movement was recorded for 30 min. Once death was established, the time of death was defined as the time point immediately following the last recorded movement. DAM2 data were analyzed using the survminer and survival R packages (Cran).

Data availability

The data described in the article are located in the figures and available upon request from David James (david.james@sydney.edu.au).

Acknowledgments—We thank the Charles Perkins Centre Research Support team, particularly Dr. Ian Garthwaite, Dr. Natalia Magarinos, Harry Simpson, Dr. Melissa Gardiner, and Dr. Macarena Rodriguez, for technical support. This research was facilitated by access to Sydney Mass Spectrometry, a core research facility at the University of Sydney.

Author contributions—J. R. K., D. J. F., and D. E. J. conceptualization; J. R. K., L.-E. Q., D. F., R. S., K. H., and C. G. formal analysis; J. R. K., D. F., G. J. C., and D. E. J. funding acquisition; J. R. K., L.-E. Q., D. F., A. Z., F. C. W., K. C. C., M. E. N., A. D.-V., S. J. H., A. H., S. I., F. S., K. S., K. H., B. V., S. R. N., A. J. H., and D. J. F. investigation; J. R. K., D. F., and S. J. H. methodology; J. R. K., D. J. F., and D. E. J. writing-original draft; J. R. K., L.-E. Q., D. F., A. Z., F. C. W., K. C. C., M. E. N., A. D.-V., S. J. H., R. S., A. H., S. I., F. S., K. S., K. H., C. G., B. V., S. R. N., A. J. H., T. S., P. J. M., G. J. C., D. J. F., and D. E. J. writing-review and editing; A. J. H., T. S., P. J. M., G. J. C., D. J. F., and D. E. J. supervision.

Funding and additional information—D. E. J. was supported by Senior Principal Research Fellowship APP1019680 and Project Grants GNT1061122 and GNT1086851 from the National Health and Medical Research Council. G. J. C. was supported by a

Professorial Research Fellowship from the University of Sydney Medical School. D. E. J. and G. J. C. were also supported by National Health and Medical Research Council Project Grant GNT1086850. J. R. K. was supported by National Health and Medical Research Council Early Career Fellowship APP1072440, an Australian Diabetes Society Skip Martin Early-Career Fellowship, a Diabetes Australia Research Program grant, and a Charles Perkins Centre Early-Career Seed Funding Grant. D. F. was funded by a Diabetes Australia Research Program Grant and Charles Perkins Centre Early-Career Seed Funding Grant. A. H. was funded by the Research on Development of New Drugs (GAPFREE) from the Japan Agency for Medical Research and Development (AMED). T. S. was funded by the AMED–CREST from AMED. A. H. and T. S. were supported by funds from the Yamagata prefectural government and the City of Tsuruoka.

Conflict of interest—The authors declare that they have no conflicts of interest with the contents of this article.

Abbreviations—The abbreviations used are: BCAA, branched chain amino acid; G3P, glycerol 3-phosphate; KRP, Krebs–Ringer phosphate; NEFA, nonesterified fatty acid; ORO, Oil Red O; TAG, triacylglyceride; DMEM, Dulbecco's modified Eagle's medium; BSF, bicarbonate-buffered, substrate-free; HSF, HEPES-buffered.

References

1. Lotta, L. A., Gulati, P., Day, F. R., Payne, F., Ongen, H., van de Bunt, M., Gaulton, K. J., Eicher, J. D., Sharp, S. J., Luan, J., De Lucia Rolfe, E., Stewart, I. D., Wheeler, E., Willems, S. M., Adams, C., *et al.* (2017) Integrative genomic analysis implicates limited peripheral adipose storage capacity in the pathogenesis of human insulin resistance. *Nat. Genet.* **49,** 17–26 CrossRef Medline
2. Rosen, E. D., and Spiegelman, B. M. (2014) What we talk about when we talk about fat. *Cell* **156,** 20–44 CrossRef Medline
3. Garvey, W. T., and Kolterman, O. G. (1988) Correlation of *in vivo* and *in vitro* actions of insulin in obesity and noninsulin-dependent diabetes mellitus: role of the glucose transport system. *Diabetes Metab. Rev.* **4,** 543–569 CrossRef Medline
4. Kraegen, E. W., Clark, P. W., Jenkins, A. B., Daley, E. A., Chisholm, D. J., and Storlien, L. H. (1991) Development of muscle insulin resistance after liver insulin resistance in high-fat-fed rats. *Diabetes* **40,** 1397–1403 CrossRef Medline
5. Turner, N., Kowalski, G. M., Leslie, S. J., Risis, S., Yang, C., Lee-Young, R. S., Babb, J. R., Meikle, P. J., Lancaster, G. I., Henstridge, D. C., White, P. J., Kraegen, E. W., Marette, A., Cooney, G. J., Febbraio, M. A., *et al.* (2013) Distinct patterns of tissue-specific lipid accumulation during the induction of insulin resistance in mice by high-fat feeding. *Diabetologia* **56,** 1638–1648 CrossRef Medline
6. Abel, E. D., Peroni, O., Kim, J. K., Kim, Y. B., Boss, O., Hadro, E., Minnemann, T., Shulman, G. I., and Kahn, B. B. (2001) Adipose-selective targeting of the GLUT4 gene impairs insulin action in muscle and liver. *Nature* **409,** 729–733 CrossRef Medline
7. Quek, L. E., Krycer, J. R., Ohno, S., Yugi, K., Fazakerley, D. J., Scalzo, R., Elkington, S. D., Dai, Z., Hirayama, A., Ikeda, S., Shoji, F., Suzuki, K., Locasale, J. W., Soga, T., James, D. E., *et al.* (2020) Dynamic ^{13}C flux analysis captures the reorganization of adipocyte glucose metabolism in response to insulin. *iScience* **23,** 100855 CrossRef Medline
8. Ma, D. K., Stolte, C., Krycer, J. R., James, D. E., and O'Donoghue, S. I. (2015) SnapShot: insulin/IGF1 signaling. *Cell* **161,** 948–948.e1 CrossRef Medline
9. Krycer, J. R., Yugi, K., Hirayama, A., Fazakerley, D. J., Quek, L. E., Scalzo, R., Ohno, S., Hodson, M. P., Ikeda, S., Shoji, F., Suzuki, K., Domanova, W., Parker, B. L., Nelson, M. E., Humphrey, S. J., *et al.* (2017) Dynamic metabolomics reveals that insulin primes the adipocyte for glucose metabolism. *Cell Rep.* **21,** 3536–3547 CrossRef Medline
10. Rodbell, M. (1964) Metabolism of isolated fat cells: I. Effects of hormones on glucose metabolism and lipolysis. *J. Biol. Chem.* **239,** 375–380 Medline
11. Bally, P. R., Cahill, G. F., Jr., Leboeuf, B., and Renold, A. E. (1960) Studies on rat adipose tissue *in vitro*: V. Effects of glucose and insulin on the metabolism of palmitate-1-C14. *J. Biol. Chem.* **235,** 333–336 Medline
12. Feller, D. D., and Feist, E. (1959) Metabolism of adipose tissue: incorporation of isoleucine carbon into lipids by slices of adipose tissue. *J. Lipid Res.* **1,** 90–96
13. Feller, D. D., and Feist, E. (1962) The conversion of leucine carbon into CO_2, fatty acids and other products by adipose tissue. *Biochim. Biophys. Acta* **62,** 40–44 CrossRef Medline
14. Rosenthal, J., Angel, A., and Farkas, J. (1974) Metabolic fate of leucine: a significant sterol precursor in adipose tissue and muscle. *Am. J. Physiol.* **226,** 411–418 CrossRef Medline
15. Green, C. R., Wallace, M., Divakaruni, A. S., Phillips, S. A., Murphy, A. N., Ciaraldi, T. P., and Metallo, C. M. (2016) Branched-chain amino acid catabolism fuels adipocyte differentiation and lipogenesis. *Nat. Chem. Biol.* **12,** 15–21 CrossRef Medline
16. Krycer, J. R., Elkington, S. D., Diaz-Vegas, A., Cooke, K. C., Burchfield, J. G., Fisher-Wellman, K. H., Cooney, G. J., Fazakerley, D. J., and James, D. E. (2020) Mitochondrial oxidants, but not respiration, are sensitive to glucose in adipocytes. *J. Biol. Chem.* **295,** 99–110 CrossRef Medline
17. Tan, S. X., Fisher-Wellman, K. H., Fazakerley, D. J., Ng, Y., Pant, H., Li, J., Meoli, C. C., Coster, A. C., Stöckli, J., and James, D. E. (2015) Selective insulin resistance in adipocytes. *J. Biol. Chem.* **290,** 11337–11348 CrossRef Medline
18. Vander Heiden, M. G., Cantley, L. C., and Thompson, C. B. (2009) Understanding the Warburg effect: the metabolic requirements of cell proliferation. *Science* **324,** 1029–1033 CrossRef Medline
19. Reitzer, L. J., Wice, B. M., and Kennell, D. (1979) Evidence that glutamine, not sugar, is the major energy source for cultured HeLa cells. *J. Biol. Chem.* **254,** 2669–2676 Medline
20. Vega, F. V., and Kono, T. (1978) Effects of insulin on the uptake of D-galactose by isolated rat epididymal fat cells. *Biochim. Biophys. Acta* **512,** 221–222 CrossRef Medline
21. Liu, L., Shah, S., Fan, J., Park, J. O., Wellen, K. E., and Rabinowitz, J. D. (2016) Malic enzyme tracers reveal hypoxia-induced switch in adipocyte NADPH pathway usage. *Nat. Chem. Biol.* **12,** 345–352 CrossRef Medline
22. Krycer, J. R., Quek, L. E., Francis, D., Fazakerley, D. J., Elkington, S. D., Diaz-Vegas, A., Cooke, K. C., Weiss, F. C., Duan, X., Kurdyukov, S., Zhou, P. X., Tambar, U. K., Hirayama, A., Ikeda, S., Kamei, Y., *et al.* (2020) Lactate production is a prioritized feature of adipocyte metabolism. *J. Biol. Chem.* **295,** 83–98 CrossRef Medline
23. Jungas, R. L. (1968) Fatty acid synthesis in adipose tissue incubated in tritiated water. *Biochemistry* **7,** 3708–3717 CrossRef Medline
24. Windmueller, H. G., and Spaeth, A. E. (1966) Perfusion in situ with tritium oxide to measure hepatic lipogenesis and lipid secretion: normal and orotic acid-fed rats. *J. Biol. Chem.* **241,** 2891–2899 Medline
25. McGarry, J. D., Takabayashi, Y., and Foster, D. W. (1978) The role of malonyl-CoA in the coordination of fatty acid synthesis and oxidation in isolated rat hepatocytes. *J. Biol. Chem.* **253,** 8294–8300 Medline
26. Mugabo, Y., Zhao, S., Seifried, A., Gezzar, S., Al-Mass, A., Zhang, D., Lamontagne, J., Attane, C., Poursharifi, P., Iglesias, J., Joly, E., Peyot, M. L., Gohla, A., Madiraju, S. R., and Prentki, M. (2016) Identification of a mammalian glycerol-3-phosphate phosphatase: role in metabolism and signaling in pancreatic β-cells and hepatocytes. *Proc. Natl. Acad. Sci. U.S.A.* **113,** E430–E439 CrossRef Medline
27. Jackson, R. M., Griesel, B. A., Gurley, J. M., Szweda, L. I., and Olson, A. L. (2017) Glucose availability controls adipogenesis in mouse 3T3-L1 adipocytes via up-regulation of nicotinamide metabolism. *J. Biol. Chem.* **292,** 18556–18564 CrossRef Medline
28. Temple, K. A., Basko, X., Allison, M. B., and Brady, M. J. (2007) Uncoupling of 3T3-L1 gene expression from lipid accumulation during adipogenesis. *FEBS Lett.* **581,** 469–474 CrossRef Medline

29. Francis, D., Krycer, J. R., Cooney, G. J., and James, D. E. (2019) A modified gas-trapping method for high-throughput metabolic experiments in *Drosophila melanogaster*. *BioTechniques* **67,** 123–125 CrossRef Medline
30. Thurmond, J., Goodman, J. L., Strelets, V. B., Attrill, H., Gramates, L. S., Marygold, S. J., Matthews, B. B., Millburn, G., Antonazzo, G., Trovisco, V., Kaufman, T. C., Calvi, B. R., and FlyBase Consortium (2019) FlyBase 2.0: the next generation. *Nucleic Acids Res.* **47,** D759–D765 CrossRef Medline
31. Graham, P., and Pick, L. (2017) *Drosophila* as a model for diabetes and diseases of insulin resistance. *Curr. Top. Dev. Biol.* **121,** 397–419 CrossRef Medline
32. Alfa, R. W., and Kim, S. K. (2016) Using *Drosophila* to discover mechanisms underlying type 2 diabetes. *Dis. Model. Mech.* **9,** 365–376 CrossRef Medline
33. Djawdan, M., Chippindale, A. K., Rose, M. R., and Bradley, T. J. (1998) Metabolic reserves and evolved stress resistance in *Drosophila melanogaster*. *Physiol. Zool.* **71,** 584–594 CrossRef Medline
34. Lee, K. P., and Jang, T. (2014) Exploring the nutritional basis of starvation resistance in *Drosophila melanogaster*. *Funct. Ecol.* **28,** 1144–1155 CrossRef
35. Liu, X., Cooper, D. E., Cluntun, A. A., Warmoes, M. O., Zhao, S., Reid, M. A., Liu, J., Lund, P. J., Lopes, M., Garcia, B. A., Wellen, K. E., Kirsch, D. G., and Locasale, J. W. (2018) Acetate production from glucose and coupling to mitochondrial metabolism in mammals. *Cell* **175,** 502–513. e13 CrossRef Medline
36. Marshall, S. (1989) Kinetics of insulin action on protein synthesis in isolated adipocytes: ability of glucose to selectively desensitize the glucose transport system without altering insulin stimulation of protein synthesis. *J. Biol. Chem.* **264,** 2029–2036 Medline
37. Stansbie, D., Denton, R. M., Bridges, B. J., Pask, H. T., and Randle, P. J. (1976) Regulation of pyruvate dehydrogenase and pyruvate dehydrogenase phosphate phosphatase activity in rat epididymal fat-pads: effects of starvation, alloxan-diabetes and high-fat diet. *Biochem. J.* **154,** 225–236 CrossRef Medline
38. Denton, R. M., and Randle, P. J. (1967) Measurement of flow of carbon atoms from glucose and glycogen glucose to glyceride glycerol and glycerol in rat heart and epididymal adipose tissue: effects of insulin, adrenaline and alloxan-diabetes. *Biochem. J.* **104,** 423–434 CrossRef Medline
39. Rodbell, M., and Jones, A. B. (1966) Metabolism of isolated fat cells: 3. The similar inhibitory action of phospholipase C (*Clostridium perfringens* α toxin) and of insulin on lipolysis stimulated by lipolytic hormones and theophylline. *J. Biol. Chem.* **241,** 140–142 Medline
40. Wise, E. M., Jr., and Ball, E. G. (1964) Malic enzyme and lipogenesis. *Proc. Natl. Acad. Sci. U.S.A.* **52,** 1255–1263 CrossRef Medline
41. Hue, L., and Taegtmeyer, H. (2009) The Randle cycle revisited: a new head for an old hat. *Am. J. Physiol. Endocrinol. Metab.* **297,** E578–E591 CrossRef Medline
42. Humphrey, S. J., Yang, G., Yang, P., Fazakerley, D. J., Stöckli, J., Yang, J. Y., and James, D. E. (2013) Dynamic adipocyte phosphoproteome reveals that Akt directly regulates mTORC2. *Cell Metab.* **17,** 1009–1020 CrossRef Medline
43. Wellen, K. E., Hatzivassiliou, G., Sachdeva, U. M., Bui, T. V., Cross, J. R., and Thompson, C. B. (2009) ATP-citrate lyase links cellular metabolism to histone acetylation. *Science* **324,** 1076–1080 CrossRef Medline
44. Fazakerley, D. J., Krycer, J. R., Kearney, A. L., Hocking, S. L., and James, D. E. (2019) Muscle and adipose tissue insulin resistance: malady without mechanism?. *J. Lipid Res.* **60,** 1720–1732 CrossRef Medline
45. Fazakerley, D. J., Naghiloo, S., Chaudhuri, R., Koumanov, F., Burchfield, J. G., Thomas, K. C., Krycer, J. R., Prior, M. J., Parker, B. L., Murrow, B. A., Stöckli, J., Meoli, C. C., Holman, G. D., and James, D. E. (2015) Proteomic analysis of GLUT4 storage vesicles reveals tumor suppressor candidate 5 (TUSC5) as a novel regulator of insulin action in adipocytes. *J. Biol. Chem.* **290,** 23528–23542 CrossRef Medline
46. Krycer, J. R., Fisher-Wellman, K. H., Fazakerley, D. J., Muoio, D. M., and James, D. E. (2017) Bicarbonate alters cellular responses in respiration assays. *Biochem. Biophys. Res. Commun.* **489,** 399–403 CrossRef Medline
47. Krycer, J. R., Fazakerley, D. J., Cater, R. J., K, C. T., Naghiloo, S., Burchfield, J. G., Humphrey, S. J., Vandenberg, R. J., Ryan, R. M., and James, D. E. (2017) The amino acid transporter, SLC1A3, is plasma membrane-localised in adipocytes and its activity is insensitive to insulin. *FEBS Lett.* **591,** 322–330 CrossRef Medline
48. Krycer, J. R., Diskin, C., Nelson, M. E., Zeng, X. Y., Fazakerley, D. J., and James, D. E. (2018) A gas trapping method for high-throughput metabolic experiments. *BioTechniques* **64,** 27–29 CrossRef Medline
49. Weir, J. M., Wong, G., Barlow, C. K., Greeve, M. A., Kowalczyk, A., Almasy, L., Comuzzie, A. G., Mahaney, M. C., Jowett, J. B., Shaw, J., Curran, J. E., Blangero, J., and Meikle, P. J. (2013) Plasma lipid profiling in a large population-based cohort. *J. Lipid Res.* **54,** 2898–2908 CrossRef Medline
50. van Winden, W. A., Wittmann, C., Heinzle, E., and Heijnen, J. J. (2002) Correcting mass isotopomer distributions for naturally occurring isotopes. *Biotechnol. Bioeng.* **80,** 477–479 CrossRef Medline
51. Herman, M. A., Peroni, O. D., Villoria, J., Schön, M. R., Abumrad, N. A., Blüher, M., Klein, S., and Kahn, B. B. (2012) A novel ChREBP isoform in adipose tissue regulates systemic glucose metabolism. *Nature* **484,** 333–338 CrossRef Medline
52. Kearney, A. L., Cooke, K. C., Norris, D. M., Zadoorian, A., Krycer, J. R., Fazakerley, D. J., Burchfield, J. G., and James, D. E. (2019) Serine 474 phosphorylation is essential for maximal Akt2 kinase activity in adipocytes. *J. Biol. Chem.* **294,** 16729–16739 CrossRef Medline
53. Chitraju, C., Mejhert, N., Haas, J. T., Diaz-Ramirez, L. G., Grueter, C. A., Imbriglio, J. E., Pinto, S., Koliwad, S. K., Walther, T. C., and Farese, R. V. Jr (2017) Triglyceride synthesis by DGAT1 protects adipocytes from lipid-induced ER stress during lipolysis. *Cell Metab.* **26,** 407–418.e3 CrossRef Medline
54. Schindelin, J., Arganda-Carreras, I., Frise, E., Kaynig, V., Longair, M., Pietzsch, T., Preibisch, S., Rueden, C., Saalfeld, S., Schmid, B., Tinevez, J. Y., White, D. J., Hartenstein, V., Eliceiri, K., Tomancak, P., *et al.* (2012) Fiji: an open-source platform for biological-image analysis. *Nat. Methods* **9,** 676–682 CrossRef Medline
55. Prabhu, A. V., Krycer, J. R., and Brown, A. J. (2013) Overexpression of a key regulator of lipid homeostasis, Scap, promotes respiration in prostate cancer cells. *FEBS Lett.* **587,** 983–988 CrossRef Medline
56. Feoktistova, M., Geserick, P., and Leverkus, M. (2016) Crystal violet assay for determining viability of cultured cells. *Cold Spring Harb. Protoc.* **2016,** pdb.prot087379 CrossRef Medline